Arsenopyrite dissolution rates in O_2-bearing solutions.

Maria P. Asta[1*], Jordi Cama[1], Carlos Ayora[1], Patricia Acero[2] and Giovanni de Giudici[3]

[1] Institute of Environmental Assessment and Water Research (IDAEA), CSIC
Jordi Girona, 18-26, Barcelona 08034, Spain

[2] Department of Earth Sciences, University of Zaragoza
Pedro Cerbuna 12, Zaragoza 50009, Spain

[3] Department of Earth Science, University of Cagliari
Via Trentino 51, Cagliari 09127, Italy

Phone +34 976761000 ext. 3159

Fax: +34 976 761106

E-mail: mpasta@unizar.es

To be submitted to: *Chemical Geology*

[*]Corresponding author; Present address; Department of Earth Sciences, University of Zaragoza, Pedro Cerbuna 12, Zaragoza 50009, Spain

ABSTRACT

Arsenopyrite dissolution was studied by means of long-term, stirred and non-stirred flow-through experiments in the pH range of 1 to 9 at 25, 50 and 70 ºC and at different input dissolved-O_2 concentrations (from 0.2 to 8.7 mg L^{-1}).

At pH lower than 4, aqueous iron, which is mainly in the ferrous form, and arsenic are stoichiometrically released. Sulphur concentrations released were lower than stoichiometrically expected (S/As <1). X-ray Photoelectron Spectroscopy (XPS) and MicroRaman Spectroscopy surface analyses on reacted and unreacted samples showed an enrichment of the reacted arsenopyrite surface in sulphur and arsenic under acidic conditions.

In the light of these results, the steady-state dissolution rates were estimated by the release of arsenic at pH < 6 and were used to derive an empirical dissolution rate law expressed as:

$$R_{arsenopyrite}(mol\,m^{-2}\,s^{-1})_{25^\circ C} = 10^{-7.41\pm0.47}\cdot a_{O_2}^{0.76\pm0.11}\cdot a_{H^+}^{-0.12\pm0.07}$$

where a_{O_2} and a_{H^+} are the activities of hydrogen ions and dissolved oxygen, respectively and their exponents were estimated from multiple linear regression of the dissolution rates. Temperature increase from 25 to 70 ˚C yields an apparent activation energy for the arsenopyrite oxidation by dissolved oxygen of 18.5±1.6 kJ mol^{-1}.

At pH > 6, aqueous iron is mainly in the ferric form and is depleted as it precipitates as Fe-oxyhydroxide onto arsenopyrite surfaces, yielding Fe/As and Fe/S less than one; between pH 7 and 9, iron depletion is complete, and sulphur released is more abundant than arsenic released, which is precipitated as As-O phases, as confirmed by MicroRaman spectroscopy. At pH 6-9, iron-oxyhydroxide phases and arsenic oxide phases upon the arsenopyrite surface provide an effective layer that reduces diffusion of dissolved oxygen and arsenopyrite

dissolution. As coating on the arsenopyrite surface becomes the rate-limiting step, the Shrinking Core Model (SCM) allows quantification of the surface dissolution rate, especially from data obtained whereas the effect of coating was still negligible. The SCM also allowed us to calculate the effective coefficient for oxygen diffusion through the coating, which can vary from 10^{-17} to $1.5 \cdot 10^{-16}$ m^2 s^{-1}. The formation of such a coating produced a decrease in arsenic and sulphur release over time and a final surface passivation.

Keywords: arsenic, arsenopyrite, dissolution, kinetics, iron coating.

1 INTRODUCTION

Inorganic aqueous As release is an environmental and human health concern worldwide (Ferguson, 1990; Aposhian et al., 2004; Rosman et al., 2004; Bunnell et al., 2007).

The arsenic content in water (surficial or groundwater) has been attributed to two main processes: desorption of arsenic previously sorbed onto the structures of Fe or Mn oxy-hydroxides, and As release by oxidation of arsenopyrite and/or As-rich pyrites in mineralized areas (Casiot et al., 2003, 2005; Frau and Ardau, 2003; Lee et al., 2005; Lee and Chon, 2006; Pfeifer et al., 2007). The former process usually occurs in aquifers where redox conditions have been changed, e.g., the arsenic contamination in the Bangladesh delta (Bhattacharya et al., 1997, 2001, 2002, 2006; Nickson et al., 1998; Routh et al., 2000; McArthur et al., 2001; Dowling et al., 2002; Smedley and Kinniburgh 2002; Anawar et al., 2003), whereas the latter process is mainly encountered in areas where As-bearing sulphides oxidize in acid mine drainage (AMD) or in near neutral to basic pH waters. In this study, we focus on the As release as arsenopyrite dissolution takes place. An important example of As mobilization is the Iberian Pyrite Belt (IPB) in the SW of Spain and S of Portugal, which is one of the most important massive sulphide provinces in the world. This area contains a large number of abandoned sulphide mines, open pits, galleries, tailings and sulphide-sludge ponds that generate creeks with acidic water with high levels of arsenic (Sánchez-Rodas et al., 2005; Sarmiento et al., 2005, 2007; Acero et al., 2006; Asta et al., 2009). Dissolved oxygen promotes dissolution of arsenopyrite (AsFeS) and arsenical pyrite ($Fe(As,S)_2$) with the consequent As release into run-off water (Williams, 2001; Lazareva et al., 2002; Smedley and Kinniburgh, 2002; Casiot et al., 2003; Frau and Ardau, 2003; Welch and Stollenwerk, 2003; Lee et al., 2005; Pfeifer et al., 2007). Other examples of arsenic contaminated groundwaters have been attributed to oxidation of arsenopyrite and As-bearing sulphides in non acidic waters at pH ranging from 7-9 in the Madrid Tertiary detrital aquifer (central Spain)

(Hernández-García and Custodio, 2004) or in groundwater with near neutral pH at Ester dome (Fairbanks, Alaska), where dissolved arsenic concentration appears to be controlled by oxidation of arsenopyrite in the near-surface environment (Verplanck et al., 2007). Smedley et al. (2007) have recently reported arsenic contamination in circumneutral-pH groundwaters in Proterozoic basement rocks in Burkina Faso. There are also other scenarios where higher pH (neutral or alkaline) is common. For example, acid generation may be artificially attenuated by adding alkaline substances to the AMD producing materials (Pérez-López et al., 2007), which results in acid neutralization. Similarly, hydrometallurgical techniques such as cyanidation have been conducted at high pH producing alkaline waters in contact with mine residues (Salzsauler et al., 2005).

The effects of different factors on the oxidative dissolution of arsenopyrite, such as temperature, Fe(III) concentration, the presence of bacteria (*Acidithiobacillus ferrooxidans*), pH and particle size have been reported in the literature, either related to aqueous chemistry studies (Breed et al., 1997; Ruitenberg et al., 1999; McGuire et al., 2001a; Craw et al., 2003; Yu et al. 2004, 2007; Tallant and McKibben, 2005, Walker et al., 2006; McKibben et al., 2008) or to arsenopyrite surface spectroscopy research, mainly by X-ray Photoelectron Spectroscopy (XPS) (Buckley and Walker, 1988; Richardson and Vaughan, 1989; Nesbitt et al., 1995; Nesbitt and Muir, 1998; Hacquard et al., 1999; Mikhlin et al., 2006). This extensive literature is indicative of the important role of arsenopyrite oxidative dissolution in different geochemical environments, from AMD to metallurgical processes, and groundwater contamination.

Recently, two thorough reviews on arsenopyrite oxidative dissolution that take into account the aforementioned studies have been published (Corkhill and Vaughan, 2009; Lengke et al., 2009). These authors indicate that discrepancies in the kinetics of arsenopyrite dissolution still exist, being induced by different experimental parameters and limited datasets. It is pointed out that there is no consensus in fundamental processes that are involved in the

overall reaction, such as: (1) formation of S layers on arsenopyrite surface, (2) dissolution stoichiometry, (3) variability in dissolution rate, (4) dissolution rate-DO dependence, (5) anomalous rate-Arrhenius behaviour.

The aim of this paper is to describe the kinetics of arsenopyrite oxidative dissolution at different oxidizing conditions by assessing the effects of environmental factors, such as pH, dissolved oxygen, sulphate content, and temperature. The main innovation of this study is that oxidation kinetic data were obtained at a long-term steady state (hundreds of hours) and a wide range of pH values, dissolved oxygen concentrations and temperature, combining the analysis of the reacted solutions with an exhaustive examination of arsenopyrite surface by means of Scanning Electron Microscopy (SEM), X-ray Photoelectron Spectroscopy (XPS) and MicroRaman Spectroscopy. In addition, the effect of iron coatings formed at high pH on arsenopyrite surface and its implication on arsenic release has been contemplated using the Shrinking Core Model (Wen, 1968). Therefore, the results from this study should be useful to improve the applicability of the empirical rate laws for As-bearing sulphide dissolution.

2 MATERIALS AND METHODS

2.1 Characterization of arsenopyrite

The arsenopyrite samples used in this study were obtained from Martinet skarn mineralization (East Pyrenees range). Some arsenopyrite fragments were crushed in an agate mortar and sieved to a size fraction below 100 μm. The powdered sample was examined by X-ray diffraction (XRD) using Cu Kα radiation over a 2θ range from 0 to 60 degrees and using a scan speed of 0.025º/18s. The XRD patterns obtained showed that the sample consisted of arsenopyrite as the main phase and a minor amount of quartz (approx. 5%). BSE image of the raw sample by Cameca SX-50 electron microprobe showed that arsenopyrite (AsFeS) was the

dominant phase with minor amounts of quartz (SiO_2) (<3%), pyrite (FeS_2) and native Bi (< 1%). The electron microprobe analysis (EMP) of the arsenopyrite atomic composition (%) was Fe 33.5±0.1, As 32.1±0.4 and S 34.4±0.4 based on 18 points, yielding an average chemical formula of $Fe_{1.0}As_{0.94}S_{1.05}$. Geometric areas were estimated from particle size distributions, determined for powdered reacted and unreacted arsenopyrite samples by using a laser diffraction size analyser (Malver, mastersize E) after ultrasonic disaggregation in ethanol. The obtained geometric areas ranged from 0.04 to 0.1 $m^2\ g^{-1}$.

BET surface areas in the same types of samples were measured using 5-point N_2 adsorption isotherms with a Micromeritics ASAP 2000 surface area analyzer and the obtained values were used for normalizing the experiments at pH<6. The final BET-determined specific surface area in those experiments varied from 0.3 to 0.7 $m^2\ g^{-1}$. These values are generally five to ten times larger than the corresponding estimated geometric areas, which is very a common finding in kinetic studies and has also been described in earlier works (White and Peterson, 1990; White and Brantley, 2003 and references therein). Unreacted and reacted powders were examined by Scanning Electron Microscopy (SEM) using a JEOL JSM-840 microscope and a field-emission scanning microscope Hitachi H-4100FE.

XPS surface examination of the initial and reacted powdered samples mounted on carbon conductive tabs was carried out with a Physical Electronics (PHI) 5500 spectrometer using a monochromatic X-ray source (with an Al Kα line of 1486.6 eV energy and 350 W) placed perpendicular to the analyzer axis and calibrated using the 3d5/2 line of Ag with a width of 0.8 eV and a binding energy of 368.3 eV. All these measurements were made in an ultra high vacuum (UHV) chamber (pressure between $6.6\cdot10^{-11}$ and $6.6\cdot10^{-12}$ atm). The analyser pass energy was 23 eV. An electron flood gun at low energies (below 25 eV) was used for charge compensation. Comparison of the relative positions of the different peaks in all the studied spectra indicated that charge shifting could be considered uniform. Spectra are shown as raw data corrected by adjusting the C1s peak (corresponding to adventitious carbon,

to a binding energy of 284.6 eV) because of the charge of the sample. Given the lack of sample cooling while acquiring the measurements, loss of elemental sulphur could occur. Therefore, the presence or absence of elemental sulphur is discussed below. Atomic concentrations of arsenic, iron and sulphur were determined from the XPS peak areas divided by atomic sensitivity factors following the Shirley background substraction. A deconvolution of the spectra into different components was carried out. Each spectrum was fitted by means of an iterative least-squares procedure with Gaussian bands. The proportion of each surface species was then determined as a function of the areas covered by each band. However, a systematic quantification of the different iron species present in the samples is not presented here because of the low signal-to-noise ratio in most of the XPS spectra for these peaks. Only the approximate position of the observed sulphur species will be described below.

Surfaces of raw arsenopyrite powder and some powders retrieved at the end of the runs at different pH were examined by MicroRaman spectroscopy, revealing traces of quartz and pyrite at the surface. MicroRaman measurements were carried out in back scattering geometry by using the polarized 514.5 nm line of an Argon-ion laser. Raman scattering measurements were performed in air at room temperature with a triple spectrometer Jobin-Yvonne Dilor integrated system with a spectral resolution of about 1 cm^{-1}. The power density at the sample was set between 5 and 10 mW mm^2. Acquisition time was between 30 and 120 s depending of the quality of the spectra that were recorded in the Stokes region by a 1200 grooves/mm grating monochromator and CCD detector system. A confocal microscope Olympus B-201 was used, with an objective 100× with 0.90 numerical aperture. The spatial resolution was less than 1 μm. In order to verify the homogeneity of the samples and the reproducibility of the reported data, all the measurements were repeated at different random points of the samples.

2.2 Solutions and analysis

All input solutions were prepared by mixing the respective analytical reagents and Millipore MQ water (18.2 $M\Omega \cdot$ cm). The analytical-grade reagents in the acidic solutions (pH 1 and 3) were HCl and H_2SO_4 (95-97%). Reagents $FeSO_4 \cdot 7H_2O$ and H_2SO_4 (95-97%) were used to prepare the 0.01M Fe^{2+} in a H_2SO_4 solution. Input solution of pH 5.7 only consisted of Millipore MQ water (18.2 $M\Omega \cdot$ cm). The solution of pH 7.6 was prepared with KH_2PO_4 and NaOH and pH 9 solution with $Na_2B_4O_7 \cdot H_2O$.

Total concentrations of As, S and Fe in input and output solutions were analyzed by Inductively Coupled Plasma Atomic Emission Spectroscopy (ICP-AES, Thermo Jarrel-Ash with CID detector and a Perkin Elmer Optima 3200 RL). Detection limits for As, Fe and S were $1.3 \cdot 10^{-6}$, $3.6 \cdot 10^{-7}$ and $3.1 \cdot 10^{-6}$ mol L^{-1}, respectively. The accuracy uncertainty in ICP-AES measurements was estimated to be around 3%. Ferrous and total dissolved iron concentrations in output solutions were determined by colorimetry using the ferrozine method (modified after To et al., 1999) in a UV–VIS HP Spectrophotometer. Fe(III) was taken as the difference between Fe(tot) and Fe(II). The quality of the results was assured by measuring several standards, blanks and duplicates. Fe(tot) concentrations matched ICP-AES results within 5%.

Input and output solutions pH was measured at experimental temperature on an unstirred aliquot of solution using a Crison meter combination electrode with temperature compensation. pH calibration was made with standards of 2, 4, 7 and 9.21 buffer solutions. The reported accuracy is ±0.02 pH units.

Redox potential was measured by an Orion combination Pt/Ag-AgCl redox electrode. The measurements were referenced to the Standard Hydrogen Electrode (*SHE*). Reliable redox potential measurements could not be systematically obtained because of considerable drifting in the recorded values with time. This drifting could be caused by the low concentrations of aqueous species in the output solutions, by the presence of $H_2S_{(g)}$ or by the absence of a clearly

dominant redox couple (Nordstrom, 2000). When it was possible to carry out the measurements the Eh was between 0.2 and 0.7 V.

2.3 Flow-through experiments

Dissolution experiments were carried out using non-stirred and stirred flow-through reactors (ca. 35 mL in volume) fully immersed in a thermostatic water-bath held at a constant temperature of 25, 50 or 70°C (± 1)°C. The reaction cells were composed of two chambers, a lower chamber of 33-mm inner diameter and an upper chamber of 26-mm inner diameter. The two chambers were separated by a fine (5 μm) nylon mesh, on which arsenopyrite powder was placed. In the stirred experiments, the magnetic bar was in contact with the powder. The dissolved oxygen concentrations in the experiments at dissolved oxygen conditions lower than those in equilibrium with a free atmosphere were achieved by enclosing the entire experimental set-up (input and output solutions, peristaltic pump, flow-through reactors and tubing) in a glove box purged with the corresponding O_2/N_2 gas mixture (4.5% O_2 in N_2 for the experiment with 2.0 mg L^{-1} of input dissolved oxygen and pure N_2 for the experiment with 0.2 mg L^{-1} of input dissolved oxygen). Input solutions were purged with the same gas mixtures filling the glove box on a regular basis to ensure the dissolved oxygen concentrations, which were checked before pumping into the reactors. Experimental oxygen partial pressure in the glove box was continuously monitored by an oxygen partial pressure detector with an accuracy of ± 0.1 % $O_{2(g)}$. The concentration of dissolved oxygen in the reacting solution was measured at steady state in some representative experiments by luminescence-based oxygen sensor using a Hach HQ10 portable dissolved oxygen meter.

To ensure that the rate of supply of oxidant (dissolved oxygen) into the cell (i.e., to the reacting mineral surface) is faster than its consumption by the rate of reaction, a series of experiments was carried out increasing the flow rate from 0.01-0.05 to 0.20-0.40 mL min^{-1}

(see Table 1). Such a high increase in flow rate did not yield an increase in dissolution rate. This fact suggests that the reaction rate is not affected by ionic transport limitations in the surrounding solution.

Steady-state conditions were considered to be attained when differences in the metal concentration of the output solution were within ± 5% for at least 200 h and four consecutive leachate samples. After the experiments, the reacted samples were collected, rinsed with double-distilled water, dried at room temperature and stored in closed microvials under controlled atmosphere until examination by Scanning Electron Microscopy (SEM) and X-Ray Photoelectron Spectroscopy (XPS), and determination of BET surface area. A schematic sketch of the experimental setting and some more details of the experimental procedure can be found elsewhere (Cama and Acero, 2005; Acero et al., 2007a,b; and Asta et al., 2010).

2.4 Calculation of dissolution rates at pH < 6

The dissolution rate in steady state, $Rate_{stst}$, (mol m^{-2} s^{-1}) was based on the release of As, Fe and S according to the expression:

$$Rate_{stst} = \frac{q(C_{j,out} - C_{j,inp})}{\nu_j A} \quad (1)$$

where q is the fluid volume flux through the system (m^3 s^{-1}), $C_{j,inp}$ and $C_{j,out}$ are the concentrations of component j (As, Fe or S) in the input and the output solutions, respectively (mol m^{-3}), ν_j is the stoichiometry coefficient of j in the dissolution reaction, and A is the reactive surface area (m^2), which in this study is calculated using the final specific surface area (m^2 g^{-1}) and the final mass (g). The error associated with the calculated dissolution rates was estimated by the Gaussian error propagation method (Barrante, 1974) to range from 12 to 25 % and it was dominated by the uncertainty of BET surface area measurements (±10-15 %).

2.5 Calculation of dissolution rates at pH > 6

At pH higher than 6, it is expected that Fe(II) released from arsenopyrite dissolution oxidizes quickly to Fe(III) (Singer and Stumm, 1970), and that Fe(III)-bearing phases precipitate on arsenopyrite surface, coating arsenopyrite grains as dissolution proceeds. This process is satisfactorily described by the shrinking core model (SCM) and was already applied to pyrite oxidation at basic pH (Nicholson et al., 1990). The model assumes spherical particle shape and, according to Wen (1968), the process of dissolution-coating can be divided into three successive steps: diffusion of reactant ($O_{2(aq)}$ in our case) from the infinite solution to the external surface of the coat, diffusion of $O_{2(aq)}$ through the coat volume and, finally, $O_{2(aq)}$-induced dissolution of the unreacted core. $O_{2(aq)}$ consumption at the core surface gives rise to a concentration gradient across the coat.

To simplify the system, we assume that diffusion in water is much faster than through the solid coat and that the unreacted core shrinks much more slowly than the time needed to reach steady-state diffusion across the coat. This means that, except in the early steps of dissolution, the coat acts as the slow barrier for the whole process, and the dissolution rate decreases as the coat accumulates.

At the onset of the experiment, when no coat is still developed, surface reaction is the step that controls the overall process. For simplicity, it is assumed that the arsenopyrite dissolution rate (mol m^{-2} s^{-1}) is linearly dependent on oxygen activity:

$$Rate = k\rho a_{O2} \quad (2)$$

where k is a mass transfer dissolution constant (m s^{-1}), ρ is the molar density of arsenopyrite (37850 mol m^{-3}), and a_{O2} is the input $O_{2(aq)}$ activity. When the coating is developed, and the overall process is controlled by oxygen diffusion through the coating, arsenopyrite dissolution depends on the oxygen flux:

(3) $$Rate = \frac{1}{\nu_{ox}} D \frac{\partial C}{\partial r}$$

where ν_{ox} is O_2 stoichiometry in the arsenopyrite dissolution reaction (see below), and D is the effective diffusion coefficient of the coating ($m^2\ s^{-1}$). The O_2 concentration gradient can be calculated as:

(4) $$\frac{\partial C}{\partial r} = \frac{C - C_s}{x}$$

Where C is the concentration of O_2 in the pore water, C_S is the concentration on the core surface, which is assumed zero, and x is the coating thickness. According to Wen (1968), the time required to react a specified molar fraction of the initial arsenopyrite, X, can be calculated on the basis of the step that controls the overall process:

- dissolution at the surface of the particle when no coating is developed (at the onset of the experiment):

(5) $$t = \frac{\nu_{ox} r_0 \rho}{kC}\left[1 - (1 - \mathrm{X})^{1/3}\right]$$

- diffusion across the coat:

(6) $$t = \frac{\nu_{ox} r_0^2 \rho}{6DC}\left[1 - 3(1 - \mathrm{X})^{2/3} + (1 - \mathrm{X})\right]$$

where r_0 is initial radius of the particle (m) and D is the effective diffusion coefficient of the coating. The total time of the overall process is obtained by summing the duration of the two steps. For each specific time, the molar fraction of arsenopyrite dissolved, X, was calculated from the accumulated mass of solute (sulphate or arsenic) released during a time span divided by the initial mass of arsenopyrite. The accumulative mass of solute was calculated as the

product of concentration per flow rate and per time increment, and the result added to the solute corresponding to the previous time span. Hence, the values of k and D were obtained for each experiment as their best fit in eqs. (5) and (6). As shown by eqs. (5) and (6), the values of k and D depend on the value of the initial radius r_0, which was estimated to be around 10 μm , as corresponds to the average particle size obtained in the determination of granulometric distribution for the initial unreacted arsenopyrite (see section 2.1).

3 RESULTS

3.1 Results based on solution chemistry

Variations with time of the output As, Fe and S concentrations in some representative flow-through experiments with different pH are depicted in Fig. 1. The duration of the experiments varied from 600 to 4500 h. In the experiments carried out at pH < 6 steady-state conditions were attained after 300-1200 h and the duration of steady state lasted for more than 300 h. In the experiments carried out at pH 7.5 steady state was not attained, and the output concentration decreased with time (Fig. 1c). Some of the experiments consisted of two to three stages with different DO concentrations while keeping pH, temperature and flow rate constant. The experimental conditions for each experiment are shown in Tables 1 and 2. The residence time in the reactors was between 1.5 and 20 h, depending on the flow rate (0.4-0.01 mL min^{-1}). Calculated total dissolved mass of arsenopyrite throughout the experiments was usually less than 10 %. As shown in Fig. 1, concentrations of arsenic, iron and sulphur in the output solutions were highest at the start of the experiments, subsequently decreasing. Initially high concentrations were probably due to the dissolution of microparticles (Fig. 2a, b), with surface areas higher than those of the bulk samples, or to the existence of external, altered layers of the ground mineral (Lasaga, 1998; Acero et al., 2007a,b,c; Acero et al., 2009).

According to Borda et al. (2004) high concentrations could be due to preferential dissolution in the early stages of the experiments. The fact that a mineral dissolves apparently faster at the start of the experiment and the fact that steady states are attained after some time (in our case 300 to 1200 h) highlight the need to carry out long term flow-through instead of short batch experiments to predict arsenopyrite dissolution in field scenarios where an extended interaction with solutions is expected.

From pH 1 to 4, sulphur concentrations in the output solutions were usually lower than As and Fe, yielding S/As lower than one, whereas output concentrations of As and Fe were practically the same, yielding Fe/As ratio close to one (Table 1). In a few experiments the Fe/As was higher than one (e.g., $1.3 < Fe/As < 1.8$). The deficit in aqueous sulphur when dissolving arsenopyrite in the pH range 2 to 4.5 in the absence of initial dissolved Fe(III) was also reported by McKibben et al. (2008), who also observed a deficit in As. Sulphur deficit in sulphide dissolution in acidic solutions has been described in earlier studies (Lochmann and Pedlik, 1995; Weisener et al., 2003, 2004; Malmström and Collin, 2004; Acero et al., 2007b); pyrite (Domènech et al., 2002); pyrrhotite (Janzen et al., 2000); galena (De Giudici and Zuddas, 2001; Cama and Acero, 2005; Cama et al., 2005). Acero et al. (2007b) during the collection of acidic output solutions detected a $H_2S_{(g)}$ odour which resulted in aqueous sulphur deficit. Although it can not be ruled out, this odour was not detected during the collection of output solutions in our study. Therefore, for experiments at pH 1 to 4, the arsenopyrite dissolution was computed from the output As and Fe concentration. As discussed below, aqueous iron was partially depleted ($Fe/As < 1$) at mildly acidic pH (4.4 to 5.8) and totally depleted at basic pH (7.5 to 9) ($[Fe]_{out}$ was below the detection limit). Arsenic output concentrations were lower than sulphur in the neutral to basic pH range (Fig. 1c,d). Therefore, for experiments at pH higher than 6, the arsenopyrite dissolution was computed from the output SO_4 concentration.

The saturation state of the output solution at the end of each experiment was calculated using the PHREEQC code (Parkhurst, 1995) and WATEQ database (Ball and Nordstrom, 2001). Data for scorodite ($FeAsO_4$ $2H_2O$) are those revised by Krause and Ettel (1988). At pH 1-3, output solutions were undersaturated with respect to native sulphur, S-bearing phases and Fe-oxy-hydroxides. In the pH range of 4.4 to 5.8, the amount of Fe(II) measured was $\leq$ 25 %. Hence, with 75 % of Fe(III) solutions were supersaturated with respect to scorodite and Fe-oxy-hydroxide phases, such as amorphous $Fe(OH)_3$, goethite and lepidocrocite. At pH > 7, although aqueous iron was depleted, calculations were run by using a very low iron concentration (10^{-7} mol L^{-1}), yielding output solutions supersaturated with respect to several iron oxy-hydroxides. A comparison of SEM photographs of samples before and after reacting in acidic and basic pH reveals the precipitation of new Fe-bearing phases at neutral and basic pH (Fig. 2). The formation of secondary iron precipitates on reacted pyrite surfaces at basic pH has been reported in earlier works (Koslides and Ciminelli, 1992; Bonnissel-Gissinger et al., 1998; Pérez-López et al., 2007).

Figure 3 plots the variation of the arsenopyrite dissolution rate with pH at 25 ˚C and dissolved O_2 concentration of 8.7 mg L^{-1} in this study and other reported works. According to our results from pH 1 to 5 the arsenopyrite dissolution rate scarcely changes with pH regardless of whether the results are based on As or Fe release (average log rate ~ -10.1 ± 0.2 mol As m^{-2} s^{-1}; see Table 1). At pH 5-6 the dissolution rate is similar to that at pH < 4. In the pH range of 7.5 to 9 the dissolution rates increase.

The dependence of arsenopyrite dissolution rate on dissolved oxygen concentration was assessed at acid pH values (Table 1). Figure 4 plots the variation in the output of As, S and Fe concentrations as dissolved oxygen concentration increased or decreased in both multistage and single experiments. The output concentrations of As, S and Fe decreased by lowering the input dissolved oxygen concentration from 8.7 to 4.5 and 0.2 mg L^{-1} (Fig. 4). The observed log DO-log rate dependence suggests that oxidation rate may be proportional to a fractional

power of the dissolved-oxygen activity (Fig. 5 a). Steady-state dissolved oxygen concentration in the reactor in all experiments was calculated based on arsenic and used to derive a rate-DO dependence in which the rate is proportional to a fractional power of the dissolved oxygen ($R = k \cdot a_{O_2}^{n}$) where *n* is the reaction order with respect to dissolved oxygen. Remarkably, the measured data in the representative experiments (Table 1) were the same (± 0.1 log DO) as the calculated DO concentrations. The reaction order with respect to oxygen estimated from multiple linear regression of the rates was 0.76±0.11. Alternatively, a non-linear fit to the rate – DO data was also possible (see Fig. 5 b). It was observed that when DO concentration excedeed $1x10^{-4}$ M, the rate became independent of DO concentration.

3.2 Results based on arsenopyrite surface spectroscopy

Atomic concentrations of iron, arsenic and sulphur at the reacted and unreacted arsenopyrite surfaces were determined by the XPS examination of the samples before and after the flow-through experiments and the obtained results are summarized in Table 3. The poor quality of the signal in the Fe2p region of the reacted arsenopyrite surfaces prevented the XPS identification of the iron surface species. The results show that, at acidic pH, arsenopyrite surface is enriched in arsenic and sulphur, whereas, at pH 4 to 9, the surface is enriched in iron and arsenic, consistently with the solution results.

An examination of the S2p spectra of arsenopyrite reacted at acidic pH and 8.7 mg L^{-1} of DO (Fig. 6a) indicates the existence of three possible species at binding energies (BE) of approximately 161.3-162.7, 163.5-164.1 and 168.6-169.1. eV. These binding energies were identified as S^{2-}, polysulphides (S_n^{2-} where $n \geq 2$), and sulphate, respectively, according to the values reported in earlier studies (Buckley and Woods, 1985; Mycroft et al. 1990; Nesbitt and Muir, 1994, 1998; Pratt et al. 1994; Nesbitt et al., 1995; Hacquard et al. 1999). The detection of elemental S on the surfaces was practically impossible (i.e., this could not be confirmed or

ruled out) owing to the technical limitations of the equipment used in the acquisition of the spectra. The examination of As3d peaks (Fig. 6b) shows a major peak at approximately 45.3 eV, which corresponds to As(V) (Nesbitt and Muir, 1998). The shoulder of the low binding energy side may indicate the contribution of As(-I) and As(II) species at binding energies of 41.3-41.7 eV and 43.3 eV, respectively (Nesbitt et al., 1995, 1998; Buckley and Walker, 1988). Spectra of arsenopyrite surface after reacting at acidic pH and low DO concentration (1.8 mg L^{-1}) showed that reduced sulphur and arsenic signals increased and the amount of the most oxidized species (As(V) and sulphates) decreased (Figs. 6 c,d).

XPS results in the pH range of 4.5-5.5 (Figs. 6e, f) show changes with respect to the results obtained at acid pH. First, at this pH the amount of surface iron is higher than in the initial sample, which can be attributed to the presence of iron precipitates (e.g., Fe(III)-hydroxides). In the S2p spectra two species are identified with an energy binding of 164.7 and 169.2 eV (Fig. 6e), which correspond to an intermediate oxysulphur (Schaufuss et al., 2000) and sulphate, respectively. In the case of As3d peak (Fig. 6f) the best fits of the spectra indicate the presence of a major contribution of As(V) and minor As(III) with peaks at 45.7 and 44 eV, respectively (Fig. 6f). In the range of pH 7-9 (Fig. 6g, h), S2p spectra show that S(-I) oxidizes mainly to polysulphides, and the As3d spectra show a shoulder with binding energies in the range of 41.8-42 that may indicate the contribution of As(-I) and a major peak at approximately 45 eV, which corresponds to As(V) (Nesbitt and Muir, 1998) (Fig. 6g, h).

MicroRaman spectra are shown in Fig. 7. Samples reacted at acidic pH (1-3) show that the most intense peaks are at 472, 219 and 150 cm^{-1} (Fig. 7a). These peaks are attributed to elemental sulphur, whereas the other noticeable peaks are due to iron oxide and As_2O_3. This seems to indicate that, under acidic conditions, native sulphur could be a dominant surface species along with a minor amount of a stable phase iron oxide. MicroRaman spectra of samples reacted at pH 7.5 (Fig. 7b) show peaks that are associated with hematite, iron oxy(hydroxide), probably goethite, as well as traces of As-O and As_2O_3 (e.g., claudetite)

(Table 4). Thus, secondary predominant surface species are pH dependent (e.g., see Brookins, 1988). It should be noted that native sulphur and iron oxy-hydroxides are very efficient Raman scatterers, i.e. the higher their crystallinity, the higher their Raman efficiency. Raman scattering involves hundreds of atomic layers below the surface.

Hence, taking into account the saturation index of the output solution and the Raman microanalysis of the solids one can conclude that iron hydroxides such as goethite may be responsible for Fe depletion at pH higher than 5. Sulphur detection by Raman spectroscopy shows the formation of elemental sulphur in significant amounts at acidic pH (1-3), although thermodynamic calculations indicate that it should not precipitate (solutions are undersaturated).

Finally, As depletion at pH > 4 could be attributed to arsenate sorption on the Fe(III)-hydroxide surface At pH < 7 the surface is positively charged, and at 7 < pH < 9, although the net surface charge is negative, positively charged sites are still available (Stumm and Morgan, 1996; Kosmulski, 2004). Accordingly, an estimation of the As sorption onto Fe-oxyhydroxide at pH range 4-9 was made on the basis of the Generalized Two layer-surface complexation model (Dzombak and Morel, 1990) using the PHREEQC code, a surface area of 600 m^2 g^{-1} (as described by Dzombak and Morel, 1990 for hydrous ferric oxide) and a surface site density of 2.3 sites nm^{-2} (Davies and Kent, 1990). Given the total amount of Fe-hydroxide, which was based on SO_4 released (<0.1 g), the maximum amount of As(III) and As(V) sorbed was less than 10^{-9} mol As (at pH < 9.5). This arsenic amount was too low to account for the As that was retained in the experiments, which was higher than 1/5 Fe (i.e. 10^{-4} mol As). Therefore, the formation of an As phase seems to be responsible for As depletion at pH>4. Based on the stoichiometry of our results (e.g., 1 < Fe/As < 2.6; Table 3), scorodite and/or pharmacosiderite or pitticite could be responsible for As depletion. Beattie and Poling (1987) showed that, at pH values greater than 7, arsenopyrite oxidation results in the formation of secondary arsenic minerals such as pitticite [$Fe_2(AsO_4)(SO_4)OH{\cdot}2H_2O$) and pharmacosiderite

421 ($2FeAsO_4 \cdot Fe(OH)_3 \cdot 5H_2O$). Similarly, Hacquard et al. (1999) observed the formation of an
422 oxidation layer composed of Fe(III) arsenite and arsenate on the arsenopyrite surface after
423 reacting with a solution of pH 10.

424 # 4 DISCUSSION

425 ## 4.1 Evolution of the arsenopyrite surface during dissolution

426 The arsenopyrite structural formula (FeAsS) has been described as $Fe^{2+}(AsS)^{2-}$ with a minor
427 contribution of $Fe^{3+}(AsS)^{3-}$ (Nesbitt et al., 1995; Shuey, 1975). Arsenic and sulphur form a
428 dianionic group by means of a covalent bond. During dissolution, iron is mainly released as
429 Fe^{2+}, and arsenic and sulphur as S^{-1} and As^{-1}, respectively, which are not stable species in
430 solution with the result that oxidation probably occurs.

431 Inspection of the reacted samples confirmed that the arsenopyrite surface undergoes
432 critical variation as a function of pH, which influenced the overall arsenopyrite oxidative
433 dissolution. At pH < 4 the overall oxidative dissolution can be simplified as (Yu et al., 2007):

434 (7) $$FeAsS(s) + \frac{11}{4}O_2(aq) + \frac{3}{2}H_2O = Fe^{2+} + H_3AsO_3(aq) + SO_4^{2-}$$

435 Hence, steady-state dissolution rates were obtained at pH < 4 based on As and Fe release
436 normalized with respect to final BET specific surface area (Table 1). The dissolution rates
437 obtained in the experiments carried out in H_2SO_4 (pH 1 and 3) were the same, within error, as
438 the rates obtained in HCl. This agreement shows that the arsenopyrite rates obtained in this
439 study are applicable to acidic environments with sulphate as the main anionic species (e.g.,
440 systems affected by acid mine drainage). Furthermore, the effect of Fe(II) on arsenopyrite rate
441 was examined at pH 1 and 8.7 mg $L^{-1}$of DO. The results showed that Fe(II) exerts little
442 influence on the arsenopyrite dissolution rate.

From pH 5 to 6, iron depletion was incomplete, yielding Fe/As and Fe/S aqueous ratios lower than one (Table 1). Likewise, incomplete arsenic depletion was observed, giving 0.81 <S/As < 1.38. At pH ranging from 7 to 9, aqueous iron was completely depleted (below the detection limit), and As depletion was higher than that at pH 5-6.

Therefore, at pH > 6 released ferrous iron rapidly oxidized to ferric iron, which precipitated as Fe-solid phases:

(8) $$Fe^{2+} + \frac{1}{4}O_2(aq) + \frac{5}{2}H_2O = Fe(OH)_3(s) + 2H^+$$

and As(III) oxidized to As(V) (eq. 9 and 10) (Walker et al., 2006):

(9) $$H_3AsO_3(aq) + \frac{1}{2}O_2(aq) = H_2AsO_4^- + H^+$$

(10) $$H_3AsO_3(aq) + \frac{1}{2}O_2(aq) = HAsO_4^{2-} + 2H^+$$

To simplify, the variable S/As aqueous ratio can be interpreted as variable proportions in the formation of scorodite and $Fe(OH)_3$ phases:

(11) $$Fe^{2+} + \frac{1}{4}O_2(aq) + HAsO_4^{2-} + \frac{3}{2}H_2O = FeAsO_4 \cdot 2H_2O(s)$$

The amorphous $Fe(OH)_3(s)$ may represent ferrihydrite, which could transform into hematite and/or goethite as pH increased (Schwertmann and Murad, 1983). This is a simplification and mixed phases as pharmacosiderite can also be possible.

The precipitated Fe(III) and As-bearing phases form a coat on the arsenopyrite grains as dissolution proceeds. As stated above, this process was modelled using the shrinking core

model (SCM). Thus, the limiting process of arsenopyrite dissolution at pH > 6 is the diffusion of $O_{2(aq)}$ through the coating, resulting in the dissolution of the unreacted core of arsenopyrite. An important parameter that governs dissolution under the SCM is the stoichiometry of $O_{2(aq)}$ in the arsenopyrite dissolution reaction (ν_{ox}), which according to the addition of eqs. 8, 9 or 10 (depending on pH) and 11 to eq. 7 is 15/4.

An example of application of the SCM that simulates the variation in sulphate concentration versus time at pH 7.5 and 0.27 mol m^{-3} $O_{2(aq)}$ is depicted in Fig. 8. As expected, the early values are sensitive to k value, whereas the influence of D increases with time. The effect of coating can be observed in the plot. After 250 h only 0.12 mol % of initial arsenopyrite was dissolved. However, if no coating had been formed the dissolution of arsenopyrite would have been 0.24 mol %. The value of the effective diffusion coefficient of the coating (m^2 s^{-1}) (D) estimated for the experiments that follow the SCM pattern varies within a range from 10^{-17}-to $1.5 \cdot 10^{-16}$ m^2 s^{-1}. No variation with temperature, pH or $O_{2(aq)}$ concentration is apparent. In pyrite dissolution experiments, Nicholson et al. (1988) estimated a D value around $3 \cdot 10^{-16}$ m^2 s^{-1} for the diffusion coefficient of O_2 through the Fe-hydroxide coating, and Huminicki and Rimstidt (2009) reported a value of $3.6 \cdot 10^{-15}$ m^2 s^{-1} for the diffusion coefficient of H_2O_2. Both values are comparable or higher than those obtained from our experiments. One reason for the discrepancy could be the dependence of D on r_0^2 (the value assumed for initial radius, eq. 6), which in our case is smaller than that reported in the pyrite case. Furthermore, the D values estimated here are 7 to 8 orders of magnitude lower than $2 \cdot 10^{-9}$ m^2 s^{-1}, the diffusion coefficient of $O_{2(aq)}$ in free water at 25°C (Han and Bartels, 1996). This difference is too large to be attributed to porosity and tortuosity of a porous medium. On the other hand, these D values are much higher than the diffusion coefficient values that are typical of solids (10^{-20} to 10^{-34} m^2 s^{-1}, Levine, 1978), but could be similar to those of poorly crystalline solids as suggested by Nicholson et al. (1988).

4.2 The effect of pH on dissolution rates

We suggest that a hydrogen ion effect on the arsenopyrite dissolution rate in this pH range is very low (Table 1; Fig. 3). This result is consistent with the insignificant pH dependence of the arsenopyrite-rate reported by Yu et al (2007) in the pH range of 2-6 (e.g., nearly zero-order dependence on pH), but is in disagreement with the pH-arsenopyrite-rate dependence reported by McKibben et al. (2008) in the range of pH 2-4.5 (Rate=$k\cdot(M_{H^+})^{0.3}$).

A slight increase of the dissolution rates is observed as pH increased. A similar basic pH-rate tendency was observed in pyrite oxidation by Williamson and Rimstidt (1994), Ciminelli and Osseo-Asare (1995a,b). In the case of arsenopyrite oxidation, Yu et al. (2007) obtained apparent arsenopyrite dissolution rates that reached a minimum near pH 7-8 followed by an increase at higher pH values.

4.3 The effect of dissolved oxygen on dissolution rates

The rates obtained at 25 ˚C at acidic pH are DO-dependent, decreasing when the dissolved oxygen concentration is diminished (Figs. 4 and 5). This type of dependence has been reported for arsenopyrite at acidic pH (Yu et al., 2007; McKibben et al., 2008) and for pyrite (Nicholson et al., 1988; Williamson and Rimstidt, 1994; Domènech et al, 2002). The reaction order of the arsenopyrite dissolution rate with respect to dissolved oxygen at acidic pH was 0.76. This value is higher than those reported by Yu et al. (2007) (0.45±0.05) at pH 5.9 and McKibben et al. (2008) (0.33±0.18) at pH 2-4.5 for arsenopyrite, and by McKibben (1984), Williamson and Rimstidt (1994) and Domènech et al. (2002) for pyrite (0.4-0.5±0.04) at pH 2-10, suggesting that arsenopyrite dissolution is more strongly influenced by DO than pyrite dissolution. In contrast to these results, Walker et al. (2006) reported rate-DO independence in the pH range from 6.3 to 6.7.

An alternative, non-linear fit to the data was also possible (see Fig.5 b), considering that when DO concentration was higher than $1x10^{-4}$ M, the rate varied barely, becoming thus DO-independent. As it was reported by Nicholson *et al.* (1988) and Domènech *et al.* (2002) for pyrite dissolution, this behaviour could be consistent with a surface mechanism that involves equilibrium adsorption-desorption. Thus, according to the non-linear behaviour, the dissolution rate-DO-dependence can be expressed as:

$$R = r_m \frac{K \cdot [O_2]}{1 + K \cdot [O_2]} \quad (12)$$

where R is the dissolution rate (mol m^{-2} s^{-1}), r_m (mol m^{-2} s^{-1}) is the rate based on maximum saturation of available surface sites, K (L mol^{-1}) is the adsorption equilibrium constant and $[O_2]$ is the dissolved oxygen concentration (mol L^{-1}). The best fit to the arsenopyrite data was obtained with the following values: $r_m = 1.2 \pm 0.1 \cdot 10^{-10}$ mol m^{-2} s^{-1} and $K = 1 \cdot 10^4$ L mol^{-1}.

4.4 The effect of temperature on the dissolution rate

The temperature dependence of dissolution rate generally follows the Arrhenius law:

$$Rate = Ae^{-E_{app}/RT} \quad (13)$$

where A is the pre-exponential factor, E_{app} is the apparent activation energy, R is the gas constant and T is the temperature (K). To obtain experimentally the apparent activation energy at different pH, experiments were carried out at 25, 50 and 70°C at acid pH by maintaining constant both the pH and dissolved O_2 concentration (Table 1 and Fig. 9). The apparent activation energy for arsenopyrite oxidation by oxygen at acid pH was 18.5 kJ mol^{-1}. Yu et al. (2007) using short-term flow reactors (6-8 h) reported E_{app} values (kJ mol^{-1}) of 43 (pH 1.8) and 57 (pH 5.9). McKibben et al. (2008) carrying out short-term batch experiments at pH 2-4.5 obtained a complicated non-Arrhenius behaviour similar to that reported by Rimstidt et al.

(1994) for arsenopyrite dissolution in iron-rich solutions (from 0 to 25 ˚C, E_{app} = 18 kJ mol^{-1} and from 25 to 60 ˚C, E_{app} = -6 kJ mol^{-1}). Our E_{app} values suggest that the overall arsenopyrite dissolution is a mixture of surface and diffusion controlled processes. Further research using rotating disk experiments would be necessary to distinguish between different reaction mechanisms.

4.5 Arsenopyrite dissolution rates

A comparison of the arsenopyrite dissolution rates obtained in this study with previously reported values is shown in Fig. 3. Table 5 gives the dissolution rates by abiotic oxidation by DO and kinetic parameters obtained in our work and in reported studies of arsenopyrite (Walker et al., 2006; Yu et al., 2007; McKibben et al., 2008). The rates of arsenopyrite dissolution obtained in this work are approximately two-three orders of magnitude slower than those reported by Yu et al. (2007) and McKibben et al. (2008), but in good agreement to that reported by Walker et al. (2006). It is important to highlight that different experimental setups and experimental conditions were used in these studies. Note that sulphide dissolution rates obtained in very short-term experiments (< 50 h) are usually one order of magnitude faster (Yu et al., 2007; McKibben et al., 2008). Indeed, on the onset of our long-term experiments apparent dissolution rates were faster than steady-state rates. Thus, the advantage of the long-term experiments is that achievement of durable steady state (> 300 h) guarantees the reaction to proceed under steady mineral-solution conditions. In line with this explanation, the dissolution rates obtained in this work are in good agreement with the rates obtained for other sulphides such as pyrite (Domènech et al. 2002), chalcopyrite (Acero et al., 2007a, 2009), sphalerite (Acero et al., 2007b), galena (Acero et al., 2007c) and marcasite (Asta et al., 2010) based on long-term experiments. Therefore, we suggest that quantification of arsenopyrite oxidation at acidic mine wastes is appropriately obtained by the long-term experiments.

5 CONCLUSIONS

In the present study, the surface chemistry and arsenopyrite dissolution were studied by means of stirred and non-stirred long term flow through experiments at a range of pH 1-9, at temperatures from 25 to 70 ºC at three different dissolved oxygen concentrations and under far-from equilibrium conditions.

On the one hand, we have shown that under the studied experimental conditions, arsenopyrite dissolution is strongly affected by dissolved oxygen and slightly affected by pH and temperature. At acidic pH, stirred and non-stirred experiments yield the same dissolution rate, and the rise in temperature yields an apparent activation energy of 18.5±1.6 kJ mol^{-1} that suggests that arsenopyrite dissolution is a mixture of surface and diffusion-controlled processes. On the other hand, the arsenopyrite surface chemistry analysis showed that, under acidic conditions arsenopyrite dissolution creates a sulphur-enriched surface layer. This layer is mainly made up by polysulphides and sulphates although the presence of elemental sulphur cannot be ruled out. However, these layers do not exert any passivating effect once the steady state is attained. At mildly acid to basic pH, precipitation of Fe phases takes place. Fe-coating grows on the mineral surface and prevents the diffusion of aqueous species through it. Thus, steady state is not attained and the output concentration (and As release) decreases with time.

These results are representative of the conditions found in remediated AMD sites using passive treatments where reacting limestone increases pH to ca. 7: Fe-layers passivate the surface of sulphides, and in addition, the high stability of Fe oxy(hydroxide) at circumneutral pH provides a considerable retention capacity of toxic metal(oid)s, such as arsenic, that are in non-admissible levels in AMD.

This aqueous and solid chemistry-based study represents a firm step towards understanding both the long-term behaviour of arsenopyrite dissolution and the implication that arsenopyrite oxidative dissolution can have in arsenic contamination into distinct waters,

583 showing the effects that dissolved oxygen and pH have on the complexity of arsenopyrite
584 dissolution kinetics.
585
586
587 *Acknowledgments.* This research was supported by the project CTM2007-66724-C02-
588 01/TECNO from the Spanish Government. MPA was financially supported by the Spanish
589 Government with a PhD fellowship. PA was financially supported by the Spanish Government
590 with a research contract from the "Juan de la Cierva" program. Albert Soler and Àngels
591 Canals from the Mineralogical Dept. of Barcelona University supplied the arsenopyrite
592 samples. We wish to express our gratitude to Javier Pérez, Vanessa Ouro, Rafel Bartrolí, Eva
593 Pelegrí, Eva Prats, Ana Dominguez and Josep Elvira for their technical assistance. We are
594 indebted to Lorenzo Calvo for his assistance in XPS analyses and to Xavier Llovet who
595 assisted in the obtainment of EMP analyses at the Technical Services of Barcelona University.
596 We also gratefully acknowledge the helpful comments and valuable suggestions made by Dr.
597 M.A. McKibben of a previous version of this manuscript. We are grateful to Dr. Josep M.
598 Soler, Dr. J.D. Rimstidt, two anonymous reviewers and associate editor Jeremy Fein for their
599 insightful comments. We thank to George Von Knorring for improving the English style of
600 this paper.
601

602

603 **6 REFERENCES**

604 Acero, P., Ayora, C., Torrentó, C., Nieto, J.M., 2006. The role of trace elements during
605 schwertmannite precipitation and subsequent transformation into goethite and jarosite.
606 Geochim. Cosmochim. Acta 70, 4130-4139.

607 Acero, P., Cama, J., Ayora, C., 2007a. Kinetics of chalcopyrite dissolution at pH 3. Eur. J.
608 Mineral. 19, 173-182.

609 Acero, P., Cama, J., Ayora, C., 2007b. Sphalerite dissolution kinetics in acidic environment.
610 Appl. Geochem 22, 1872-1883.

611 Acero, P., Cama, J., Ayora, C., 2007c. Rate law for galena dissolution in acidic environment.
612 Chem. Geol. 245, 219-229.

613 Acero, P., Cama, J., Ayora, C., Asta, M.P. 2009. Chalcopyrite dissolution rate law from pH 1
614 to 3. Geol. Acta 7, 389-397.

615 Anawar, H.M., Akai, J., Komaki, K., Terao, H., Yoshioka, T., Ishizuka, T., Safiullah, S., Kato,
616 K., 2003. Geochemical occurrence of arsenic in groundwater of Bangladesh: sources and
617 mobilization processes. J. Geochem. Explor. 77, 109-131.

618 Aposhian, H.V., Zakharyan, R.A., Avram, M.D., Sampayo-Reyes, A., Wollenberg, M.L.,
619 2004. A review of the enzymology of arsenic metabolism and a new potential role of
620 hydrogen peroxide in the detoxication of the trivalent arsenic species. Toxicol. Appl.
621 Pharmacol. 198, 327-335.

622 Asta, M.P., Ayora C., Roman-Ross G., Cama, J., Acero P. , Gault, A.G., Charnock, J.M., and
623 Bardelli, F. 2009. Natural attenuation of arsenic in the Tinto Santa Rosa acid stream
624 (Iberian Pyritic Belt, SW Spain): the role of iron precipitates. Chemical Geology, 271, 1-
625 12.

626 Asta, M.P., Cama, J., Acero, P. 2010. Dissolution kinetics of marcasite at acidic pH. Eur. J.
627 Mineral. doi: 10.1127/0935-1221/2010/0022-1981.

628 Ball, J., Nordstrom, D.K., 2001. User's manual for WATEQ4F with revised thermodynamic
629 database and test cases for calculating speciation of major, trace and redox elements in
630 natural waters. U.S. Geological Survey Water-Resources Investigation Report 91–183.

631 Barrante, J.R., 1974. Applied Mathematics for Physical Chemistry. Prentice-Hall, Inc.

632 Beattie, M.J.V., Poling, G.W., 1987. A Study of the Surface Oxidation of Arsenopyrite Using
633 Cyclic Voltammetry. Int. J. Miner. Process. 20(1-2), 87-108.

634 Bersani, D., Lottici, P.P., Montenero, A., 1999. Micro-raman investigation of iron oxide films
635 and powders produced by sol-gel syntheses. J. Raman Spectrosc. 30, 355-360.

636 Bhattacharya, P., Chatterjee, D., Jacks, G., 1997. Occurrence of arsenic contaminated
637 groundwater in alluvial aquifers from Delta Plains, eastern India: options for safe drinking
638 water supply. Int. J. Water. Resour Manage. 13, 79-92.

639 Bhattacharya, P., Jacks, G., Jana, J., Sracek, A., Gustafsson, J.P., Chatterjee, D. 2001.
640 Geochemistry of the Holocene alluvial sediments of Bengal Delta Plain from West Bengal,
641 India: implications on arsenic contamination in groundwater. In Groundwater Arsenic
642 Contamination in the Bengal Delta Plain of Bangladesh (ed. G. Jacks, P. Bhattacharya, and
643 A.A. Khan), pp. 21-40. TRITA-AMI Report 3084, KTH Spec Pub, KTH.

644 Bhattacharya, P., Jacks, G., Ahmed, K.M., Khan, A.A., Routh, J., 2002. Arsenic in
645 groundwater of the Bengal Delta Plain aquifers in Bangladesh. Bull. Env. Cont. Toxicol.
646 69, 538-545.

647 Bhattacharya, P., Ahmed, K. M., Hasan, M.A., Broms, S., Fogelström, J., Jacks, G., Sracek,
648 O., von Brömssen, M., Routh, J., 2006. Mobility of arsenic in groundwater in a part of
649 Brahmanbaria district, NE Bangladesh. In Managing Arsenic in the Environment: From
650 Soil to Human Health (ed. E. S. R. Naidu, G. Owens, P. Bhattacharya, P.Nadebaum), pp.
651 95-115. CSIRO, Melbourne, Australia.

652 Bonnissel-Gissinger, P., Alnot, M., Ehrhardt, J. J., and Behra, P., 1998. Surface oxidation of
653 pyrite as a function of pH. Environ. Sci. Technol. 32, 2839-2845.

654 Borda, M. J., Strongin, D.R., Schoonen, M.A., 2004. A vibrational spectroscopic study of the
655 oxidation of pyrite by molecular oxygen. Geochim. et Cosmochim. Acta 68, 1807-1813.

656 Breed, A.W., Harrison, S.T.L., Hansford, G.S., 1997. A preliminary investigation of the ferric
657 leaching of a pyrite/arsenopyrite flotation concentrate. Miner. Eng. 10, 1023-1030.

658 Bonnissel-Gissinger, P., Alnot, M., Ehrhardt, J.J., Behra, P., 1998. Surface oxidation of pyrite
659 as a function of pH. Environ. Sci. Technol. 32, 2839-2845.

660 Brookins, D.G., 1988. Eh-pH diagrams for geochemistry. Springer-Verlag, Berlin.

661 Buckley, A.N., Walker, G.W., 1988. The surface-composition of arsenopyrite exposed to
662 oxidizing environments. Appl. Surf. Sci. 35, 227-240.

663 Buckley, A.N., Woods, R., 1985. X-Ray photoelectron spectroscopy of oxidized pyrrothite
664 surfaces. I Expose to air. Appl. Surf. Sci. 22, 280-287.

665 Bunnell, J.E., Finkelman, R.B., Centeno, J.A., Selinus, O., 2007. Medical geology: a globally
666 emerging discipline. Geol. Acta 5, 273-281.

667 Cama, J., Acero, P., 2005. Dissolution of minor sulphides present in a pyritic sludge at pH 3
668 and 25 ºC. Geol. Acta 3, 15-26.

669 Cama, J., Acero, P., Ayora, C., Lobo, A., 2005. Galena surface reactivity at acidic pH and
670 25ºC based on flow-through and in situ AFM experiments. Chem. Geol. 214, 309-330.

671 Casiot, C., Leblanc, M., Bruneel, O., Personne, J.C., Koffi, K., Elbaz-Poulichet F.O., 2003.
672 Geochemical processes controlling the formation of As-rich waters within a tailings
673 impoundment (Carnoulès, France). Aquat. Geochem. 9, 273-290.

674 Casiot, C., Lebrun, S., Morin, G., Bruneel, O., Personne, J.C., Elbaz-Poulichet, F.O., 2005.
675 Sorption and redox processses controlling arsenic fate and transport in a stream impacted
676 by acid mine drainage. Sci. Total Environ. 347, 122-130.

677 Ciminelli, V.S.T., Osseo-Asare, K., 1995a. Kinetics of pyrite oxidation in sodium carbonate
678 solutions. Metall. Mater. Trans. B 26, 209-218.

679 Ciminelli V.S.T., Osseo-Asare K., 1995b. Kinetics of Pyrite Oxidation in Sodium-Hydroxide
680 Solutions. Metall. Mater. Trans. B 26, 677-685.

681 Corkhill, C.L., Vaughan, D.J., 2009. Arsenopyrite oxidation - A review. Appl. Geochem. 24,
682 2342-2361.

683 Costa, M.C., Botelho Do Rego, A.M., Abrantes, L.M., 2002. Characterization of a natural and
684 an electro-oxidized arsenopyrite: A study on electrochemical and X-ray photoelectron
685 spectroscopy. Int. J. Miner. Process. 65, 83-108.

686 Craw, D., Falconer, D., Youngson, J.H., 2003. Environmental arsenopyrite stability and
687 dissolution: theory, experiment, and field observations. Chem. Geol. 199, 71-82.

688 Davies, J.A,. Kent, D.B., 1990. Surface complexation modelling in aqueous geochemistry.
689 Rev. Mineral. Geochem. 23, 177-260.

690 De Giudici, G., Zuddas, P., 2001. In situ investigation of galena dissolution in oxygen
691 saturated solution: evolution of surface features and kinetic rate. Geochim. Cosmochim.
692 Acta 65, 1381-1389.

693 Domènech, C., de Pablo, J., Ayora, C., 2002. Oxidative dissolution of pyritic sludge from the
694 Aznalcollar mine (SW Spain). Chem. Geol. 190, 339-353.

695 Dowling, C.B., Poreda, R.J., Basu, A.R., Peters, S.L., 2002. Geochemical study of arsenic
696 release mechanisms in the Bengal Basin groundwater. Water Resour. Res. 38, 1-18.

697 Dzombal, D.A., Morel, F.M.M., 1990. Surface complexation modeling. Wiley-Interscience,
698 New York.

699 Ferguson, J.E., 1990. The heavy elements-chemistry, environmental impact and health effects.
700 Pergamon Press.

701 Flynn, E.J., Solin, S.A., Papatheodorou, G.N., 1976. Vibrational excitations of As2O3. II.
702 crystalline phases. Phys. Rev. B 13, 1752-1758.

703 Frau, F., Ardau, C., 2003. Geochemical controls on arsenic distribution in the Baccu Locci
704 stream catchment (Sardinia, Italy) affected by past mining. Appl. Geochem. 18, 1373-
705 1386.

706 Hacquard, E., Bessiere, J., Alnot, M., Ehrhardt, J.J., 1999. Surface spectroscopic study of the
707 adsorption of Ni(II) on pyrite and arsenopyrite at pH 10. Surf. Interface Anal. 27, 849-860.

708 Han, P., Bartels, D.M., 1996. Temperature dependence of oxygen difusión in H2O and D2O.
709 J. Phys. Chem., 100, 5597-5602.

710 Hernández-García, M.E., Custodio, E., 2004. Natural baseline quality of Madrid Tertiary
711 detrital aquifer groundwater (Spain): A basis for aquifer management. Environ. Geol. 46,
712 173-188.

713 Huminicki, D. M. C. and Rimstidt, J. D., 2009. Iron oxyhydroxide coating of pyrite for acid
714 mine drainage control. Applied Geochemistry 24, 1626-1634.

715 Janzen, M.P., Nicholson, R.V., Scharer, J.M., 2000. Pyrrhotite reaction kinetics: Reaction
716 rates for oxidation by oxygen, ferric iron, and for nonoxidative dissolution. Geochim.
717 Cosmochim. Acta 64, 1511-1522.

718 Koslides, T., Ciminelli, V.S.T., 1992. Pressure Oxidation of Arsenopyrite and Pyrite in
719 Alkaline-Solutions. Hydrometallurgy 30, 87-106.

720 Kosmulski, M., 2004. pH dependent surface charging and points of zero charge II. Update. J.
721 Colloid and Interface Sci. 275, 214-224.

722 Krause, E., Ettel, V.A., 1988. Solubility and stability of scorodite, $FeAsO_4$ $2H_2O$: New data
723 and further discussion. Am. Mineral. 73, 850-854.

724 Lasaga, A.C., 1998. Kinetic Theory in the Earth Sciences. Princeton University Press, New
725 Jersey.

726 Lazareva, E.V., Shuvaeva, O.V., Tsimbalist, V.G., 2002. Arsenic speciation in the tailings
727 impoundment of a gold recovery plant in Siberia. Geochem.: Explor. Environ. Anal. 2,
728 263-268.

729 Lee, J.S., Chon, H.T., 2006. Hydrogeochemical characteristics of acid mine drainage in the
730 vicinity of an abandoned mine, Daduk Creek, Korea. J. Geochem. Explor. 88, 37-40.

731 Lee, P.K., Kang, M.J., Choi, S.H., Touray, J.C., 2005. Sulphide oxidation and the natural
732 attenuation of arsenic and trace metals in the waste rocks of the abandoned Seobo tungsten
733 mine, Korea. Appl. Geochem. 20, 1687-1703.

734 Lengke, M.F., Sanpawanitchakit, C., Tempel, R.N., 2009. The oxidation and dissolution of
735 arsenic-bearing sulfides. Can. Mineral., 47, 593-613.

736 Levine, I.N., 1978. Physical Chemistry. McGraw Hill, New York.

737 Lochmann, J., Pedlik, M., 1995. Kinetic Anomalies of Dissolution of Sphalerite in Ferric
738 Sulphate-Solution. Hydrometallurgy 37, 89-96.

739 Malmström, M.E., Collin, C., 2004. Sphalerite weathering kinetics: effect of ph and particle
740 size. Proc. 11th Symp. Water-Rock Interaction, 849-852.

741 Martens, W., Frost, R.L., Kloprogge, J.T., 2003a. Raman spectroscopy of synthetic erythrite,
742 partially dehydrated erythrite and hydrothermally synthesized dehydrated erythrite. J.
743 Raman Spectrosc. 34, 90-95.

744 Martens, W., Frost, R.L., Kloprogge, J.T., Williams, P.A., 2003b. The basic copper arsenate
745 minerals olivenite, cornubite, cornwarlite, and clinoclase: An infrared emission and raman
746 spectroscopic study. Am. Mineral. 88, 501-508.

747 McArthur, J.M., Ravencroft, P., Safiullah, S., Thirlwall, M.F., 2001. Arsenic in groundwater:
748 testing pollution mechanism for sedimentary aquifers in Bangladesh. Water Resour. Res.
749 37, 109-117.

750 McGuire, M.M., Banfield, J.F., Hamers, R.J., 2001a. Quantitative determination of elemental
751 sulphur at the arsenopyrite surface after oxidation by ferric iron: mechanistic implications.
752 Geochem. Trans. 2, 25-29.

753 McGuire, M.M., Jallad, K.N., Ben-Amotz, D., Hamers, R.J., 2001b. Chemical mapping of
754 elemental sulphur on pyrite and arsenopyrite surfaces using near-infrared raman imaging
755 microscopy. Appl. Surf. Sci. 178, 105-115.

McKibben, M.A., 1984 Kinetics of aqueous oxidation of pyrite by ferric ion, oxygen and hydrogen peroxide from pH 1-4 and 20-40 ºC. Ph.D. Thesis, Pennsylvania State University, U.S.A.

McKibben, M.A., Tallant, B.A., Del Angel, J.K., 2008. Kinetics of inorganic arsenopyrite oxidation in acidic aqueous solutions. Appl. Geochem. 23, 121-135.

Mikhlin, Y.L., Romanchenko, A.S., Asanov, I.P., 2006. Oxidation of arsenopyrite and deposition of gold on the oxidized surfaces: A scanning probe microscopy, tunneling spectroscopy and XPS study. Geochim. Cosmochim. Acta 70, 4874-4888.

Mycroft, J.R., Bancroft, G.M., McIntyre, N.S., Lorimer, J.W., Hill, I.R., 1990. Detection of Sulphur and Polysulphides on Electrochemically Oxidized Pyrite Surfaces by X-Ray Photoelectron-Spectroscopy and Raman-Spectroscopy. J. Electroanal. Chem. 292, 139-152.

Nesbitt, H.W., Muir, I.J., 1994. X-Ray Photoelectron Spectroscopic Study of a Pristine Pyrite Surface Reacted with Water-Vapor and Air. Geochim. Cosmochim. Acta 58, 4667-4679.

Nesbitt, H.W., Muir, I.J., 1998. Oxidation states and speciation of secondary products on pyrite and arsenopyrite reacted with mine waste waters and air. Mineral. and Petrol. 62, 123-144.

Nesbitt, H.W., Muir, L.J., Pratt, A.R., 1995. Oxidation of Arsenopyrite by Air and Air-Saturated, Distilled Water, and Implications for Mechanism of Oxidation. Geochim. Cosmochim. Acta 59(9), 1773-1786.

Nicholson, R.V., Gilham, R.V., Reardon, E.J., 1988. Pyrite oxidation in carbonate-buffered solutions:1. experimental kinetics. Geochim. Cosmochim. Acta 52, 1077-1085.

Nicholson, R.V., Gilham, R.V., Reardon, E.J., 1990. Pyrite oxidation in carbonate-buffered solutions: 2. rate control by oxide coatings. Geochim. Cosmochim. Acta 54, 395-402.

Nickson, R., McArthur, J., Burgess, W., Ahmed, K.M., Ravenscroft, P., Rahman, M., 1998. Arsenic poisoning of groundwater in Bangladesh. Nature 395, 338.

Nordstrom, D., 2000. Aqueous Redox Chemistry and the Behaviour of Iron in Acid Mine Waters. In Proceedings of the 18 Workshop on Monitoring Oxidation-Reduction Processes for Groundwater Restoration. (eds. R.T. Wilkin, R.D. Ludwig and R.G. Ford), pp. 43–47. Environmental Protection Agency, EPA /600/R-02/002.

Parkhusrt, D., 1995. User's guide to PHREEQC: A computer program for speciation, reaction path, advective-transport, and inverse geochemical calculations. US Geological Survey Water Resources Investigation Report, 95-4227, Lakewood, Colorado, 143 pp.

Pérez-López, R., Cama, J., Nieto, J.M., Ayora, C., 2007. The iron-coating role on the oxidation kinetics of a pyritic sludge doped with fly ash. Geochim. Cosmochim. Acta 71, 1921-1934.

Pfeifer, H.R., Häussermann, A., Lavanchy, J.C., Halter. W., 2007. Distribution and behavior of arsenic in soils and waters in the vicinity of the former gold-arsenic mine of Salanfe, Western Switzerland. J. Geochem. Explor. 93, 121-134.

795 Pratt, A.R., Nesbitt, H.W., Muir, I.J., 1994. Generation of Acids from Mine Waste - Oxidative
796 Leaching of Pyrrhotite in Dilute H_2SO_4 Solutions at pH 3.0. Geochim. Cosmochim. Acta
797 58, 5147-5159.

798 Richardson, S., Vaughan, D.J., 1989. Arsenopyrite - a Spectroscopic Investigation of Altered
799 Surfaces. Mineral. Mag. 53, 223-229.

800 Rosman, T.G., Uddin, A.N., Burns, F.J., 2004. Evidence that arsenic acts as a carcinogen in
801 skin cancer. Toxicol. Appl. Pharmacol. 198, 394-404.

802 Routh, J., Bhattacharya, P., Jacks, G., Ahmed, K.M., Khan, A.A., Rahman, M.M., 2000.
803 Arsenic geochemistry of Tala groundwater and sediments from Satkhira District,
804 Bangladesh. Eos. Trans. Am. Geophys. Union 81, 550.

805 Ruitenberg, R., Hansford, G.S., Reuter, M.A., Breed, A.W., 1999. The ferric leaching kinetics
806 of arsenopyrite. Hydrometallurgy 52, 37-53.

807 Salzsauler, K.A., Sidenko, N.V., Sherriff, B.L., 2005. Arsenic mobility in alteration products
808 of sulphide-rich, arsenopyrite-bearing mine wastes, snow lake, manitoba, Canada. Appl.
809 Geochem. 20, 2303-2314.

810 Sánchez-Rodas, D., Gomez-Ariza, J.L., Giraldez, I., Velasco, A., Morales, E., 2005. Arsenic
811 speciation in river and estuarine waters from southwest Spain. Sci. Total Environ. 345,
812 207-217.

813 Sarmiento, A.M., Casiot, C., Nieto, J.M., Elbaz-Poulichet, F., Olias, M., 2005. Seasonal
814 variations in Fe and As speciation and mobility in waters affected by acid mine drainage in
815 the Odiel river basin (Huelva, Spain). Geogaceta 37, 115-118.

816 Sarmiento, A.M., Oliveira, V., Gómez-Ariza, J.L., Nieto, J.M., Sánchez-Rodas, D., 2007. Diel
817 cycles of arsenic speciation due to photooxidation in acid mine drainage from the iberian
818 pyrite belt (SW, Spain). Chemosphere 66, 677-683.

819 Schaufuss, A.G., Nesbitt, H.W., Scaini, M.J., Hoechst, H., Bancroft, M.G., Szargan, R., 2000.
820 Reactivity of surface sites on fractured arsenopyrite (FeAsS) toward oxygen. Am. Mineral.
821 85, 1754-1766.

822 Schwertmann, U., Murad, E., 1983. The effect of pH on the formation of goethite and
823 hematite from ferrihydrite. Clays Clay Miner. 31, 277-284.

824 Shuey, R.T., 1975. Arsenopyrite FeAsS. In Semiconducting Ore Minerals. Elsevier, New
825 York, USA.

826 Singer, P.C., Stumm, W., 1970. Acidic mine drainage: the rate determining step. Science, 167,
827 1121-1123.

828 Smedley, P.L., Kinniburgh, D.G., 2002. A review of the source, behaviour and distribution of
829 arsenic in natural waters. Appl. Geochem. 17, 517-568.

830 Smedley, P. L., Knudsen, J., Maiga, D., 2007. Arsenic in groundwater from mineralized
831 Proterozoic basement rocks of Burkina Faso. Appl. Geochem. 22, 1074-1092.

832 Stumm, W. and Morgan, J.J (1996) Aquatic chemistry. Chemical Equilibria and Rates in
833 Natural Waters. Wiley Interscience, New York.

834 Tallant, B.A., McKibben, M.A., 2005. Arsenic mineral kinetics: Arsenopyrite oxidation.
835 Geochim. Cosmochim. Acta 69, A820-A820.

836 To, T., Nordstrom, K.D., Cunningham, K., Ball, J., and McCleskey, B., 1999. New method for
837 the direct determination of dissolved Fe(III) concentration in acid mine waters. Environ.
838 Sci. Technol. 33, 807-813.

839 Verplanck, P.L., Mueller, S.H., Goldfarb, R.J., Nordstrom, D.K., Youcha, K., 2007.
840 Geochemical controls of elevated arsenic concentrations in groundwater, Ester Dome,
841 Fairbanks disctrict, Alaska. Chem. Geol. 255, 160-172.

842 Walker, F.P., Schreiber, M.E., Rimstidt, J.D., 2006. Kinetics of arsenopyrite oxidative
843 dissolution by oxygen. Geochim. Cosmochim. Acta 70, 1668-1676.

844 Weisener, C., Smart, R., Gerson, A., 2003. Kinetics and mechamisms of the leaching of low
845 Fe sphalerite. Geochim. Cosmochim. Acta 67, 823-830.

846 Weisener, C., Smart, R., Gerson, A., 2004. A comparison of the kinetics and mechanism of
847 acid leaching of sphalerite containing low and high concentrations of iron. J. Miner.
848 Process. 74, 239-249.

849 Welch, A.H., Stollenwerk, K.G.E., 2003. Arsenic in Ground Water: Geochemistry and
850 Occurrence. Kluwer Academic Publishers.

851 Wen, C.Y., 1968. Noncatalytic solid-fluid reaction models. Ind. Eng. Chem. 60, 34-54.

852 White, A. F. and Peterson, M. L., 1990. Role of reactive-surface-area characterization in
853 geochemical kinetic models. In: Melchior, D. C. and Bassett, R. L. Eds.) *ACS Symposium*
854 *Series 416, Chemical Modeling of Aqueous Systems II*. American Chemical Society,
855 LosAngeles, California.

856 White, A. & Brantley, S., 2003.The effect of time on the weathering of silicate minerals: why
857 do weathering rates differ in the laboratory and field? Chem. Geol., 202, 479-506.

858 Williams, M., 2001. Arsenic in mine waters: an international study. Environ. Geol. 40, 267-
859 278.

860 Williamson, M.A., Rimstidt, J.D., 1994. The Kinetics and Electrochemical Rate-Determining
861 Step of Aqueous Pyrite Oxidation. Geochim. Cosmochim. Acta 58, 5443-5454.

862 Yu, Y., Zhu, Y., Williams-Jones, A.E., Gao, Z., Li, D., 2004. A kinetic study of the oxidation
863 of arsenopyrite in acidic solutions: implications for the environment. Appl. Geochem. 19,
864 435-444.

865 Yu, Y., Zhu, Y., Gao, Z., Gammons, C.H., Li, D., 2007. Rates of arsenopyrite oxidation by
866 oxygen and Fe(III) at pH 1.8-12.6 and 15-45 ºC. Environ. Sci. Technol. 41, 6460-6464.

867

TITLES OF TABLES

Table 1. Experimental conditions and arsenopyrite dissolution rates based on steady-state values at acidic pH.

Table 2. Experimental conditions and dissolution rates obtained by the SCM at neutral and basic pH. D is the diffusion coefficient for O_2 through the coating.

Table 3. Results obtained from X-ray Photoelectron Spectroscopy (XPS) determinations on the initial and reacted arsenopyrite samples. Surface stoichiometry is represented by molar ratios.

Table 4. Results obtained from micro-Raman spectra on the initial and reacted arsenopyrite samples (AsFeS means arsenopyrite).

Table 5. Arsenopyrite dissolution rate laws obtained in earlier studies and in the present work.

FIGURE CAPTIONS

Fig. 1. Variation in total iron (grey rhombi), arsenic (black rombhi) and sulphur (circles) as a function of time in arsenopyrite representative experiments at different pH and 8.7 mgL^{-1} of input O_2-dissolved and 25 °C. Initial concentrations for the experiments are not depicted for the sake of significance of the vertical scale at basic pH, and iron concentration is not depicted because it was below detection limit.

Fig. 2. SEM images of (a) freshly ground arsenopyrite with attached microparticles on the surfaces; (b) reacted arsenopyrite sample at pH 1 and 25ºC, microparticles on the grains mostly dissolved; (c) reacted arsenopyrite sample at pH 5.5, precipitates upon grains of arsenopyrite; and (d) arsenopyrite grain with precipitates on surface after reacting at pH 7.5.

Fig. 3. Comparison of arsenopyrite oxidative dissolution rates versus pH obtained at 25ºC and atmospheric conditions in the present study and in reported works (see also Table 5 for the experimental set up details). St-St means steady state conditions and SCM corresponds to the dissolution rates obtained using the Shrinking Core Model (SCM).

Fig. 4. Variation in output As, S and Fe concentration as a function of time and dissolved oxygen at 25ºC and at pH 1 (a), at pH 3 (b). In (a) and (b) vertical lines delineate the different stages with different input DO concentration at each stage.

Fig. 5. Arsenopyrite dissolution rate dependence on dissolved oxygen at pH 1 and 25ºC. Log arsenopyrite dissolution rate vs. log DO in the reactor calculated (a); dissolution rate vs. dissolved oxygen (b).

Fig. 6. Curve fitted S2p and As3d spectra of arsenopyrite representative samples dissolved at 25ºC, 8.7 mg L^{-1} input DO and pH 3 (a) and (b); at 1.8 mg L^{-1} input DO and pH 3 (c) and (d); 8.7 mg L^{-1} input DO and pH 5.6 (e) and (f) and); 8.7 mg L^{-1} input DO and pH 7.

Fig. 7. MicroRaman spectra of arsenopyrite samples reacted at 8.7 mg L^{-1} DO at 25 ˚C and at pH 3 (a); and pH 7 (b).

Fig. 8. Evolution of the molar fraction of arsenopyrite dissolved, *X*, versus time in the experiment ASP-22 (see Table 2). The curves are the plot of the process controlled by the surface dissolution step (k control; eq. 2), by the diffusion across the coating step (D control; eq. 3), and by the SCM model (the addition eq. 2 and 3).

Fig. 9. Arrhenius plot of arsenopyrite dissolution rates obtained at acidic pH (a) and 8.7 mg L^{-1} input DO. The apparent activation energy is obtained in kJ mol^{-1}.

Figure 1a

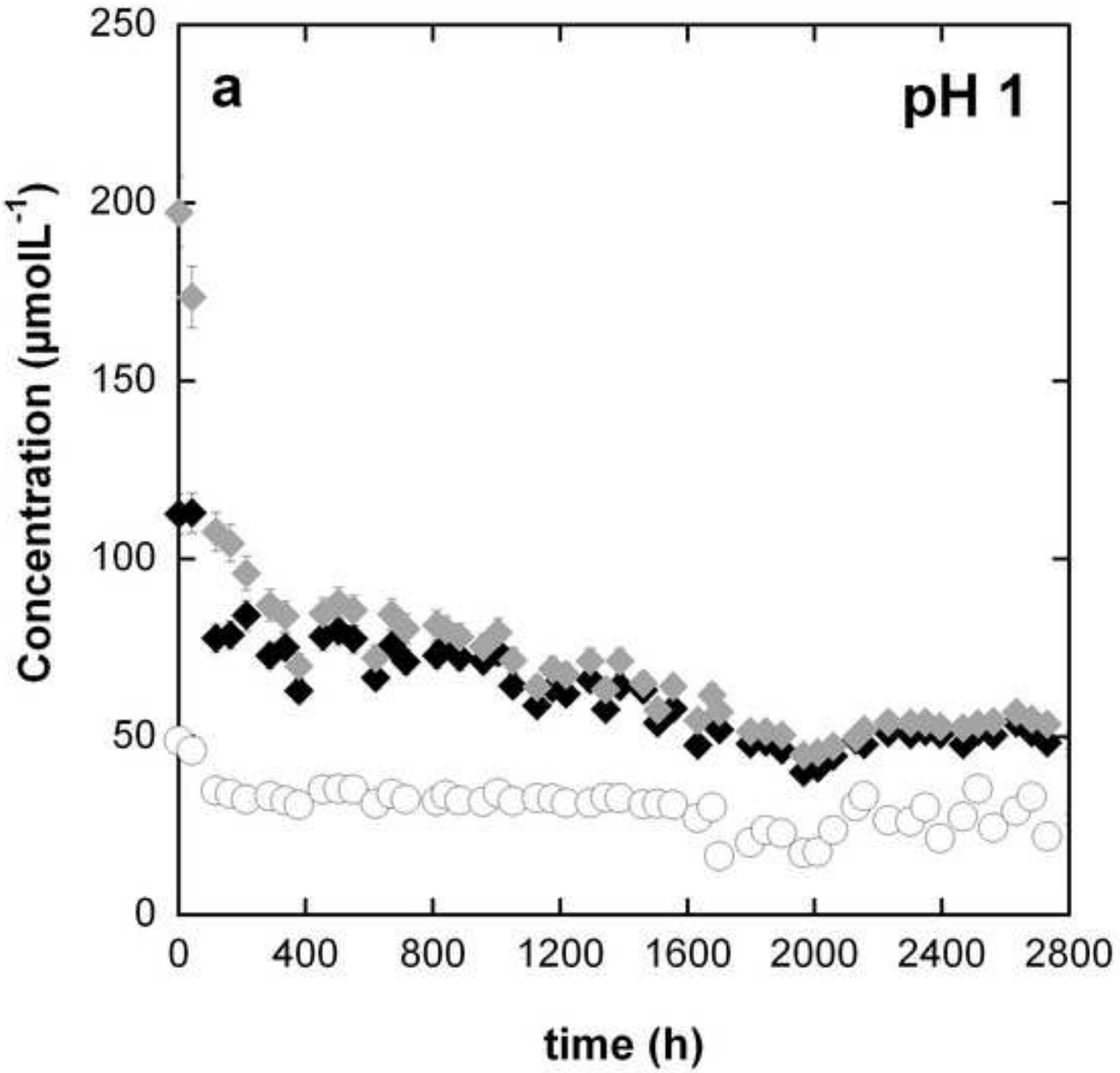
a
pH 1
Concentration (µmolL-1)
250
200
150
100
50
0
0
400
800
1200
1600
2000
2400
2800
time (h)

Figure 1b

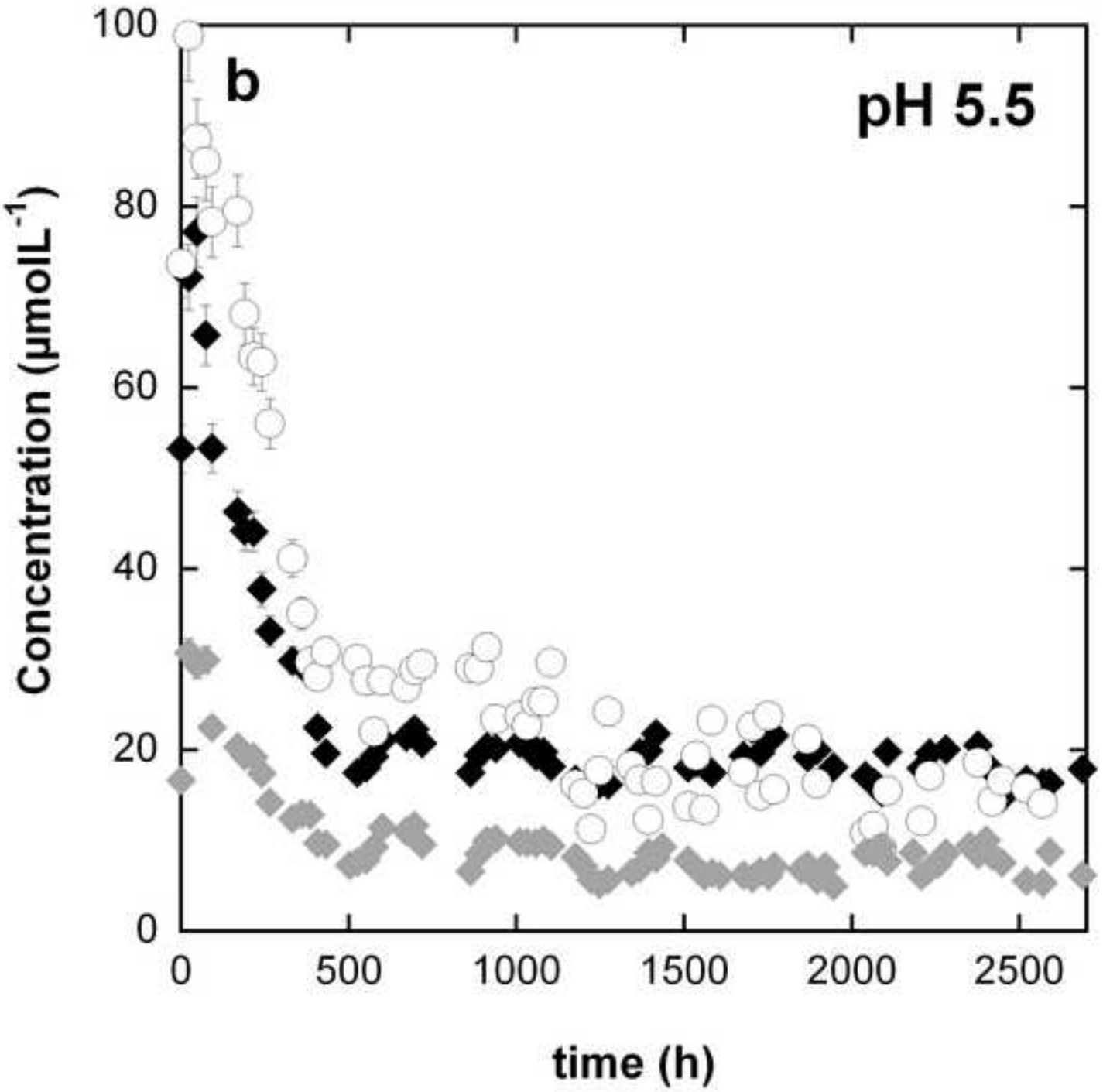
b
pH 5.5
Concentration (µmolL-1)
time (h)
0
20
40
60
80
100
0
500
1000
1500
2000
2500

Figure 1c

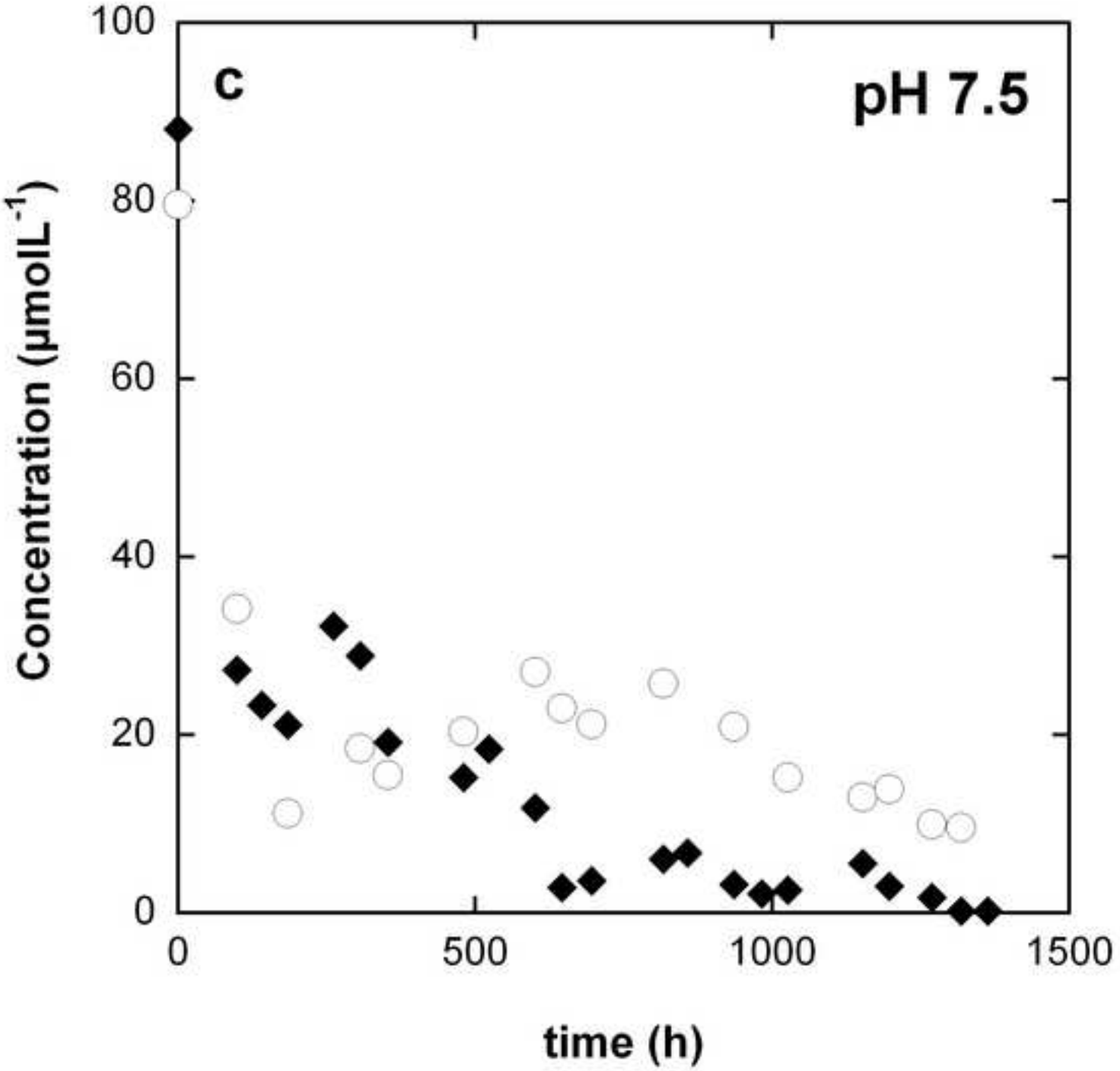
c
pH 7.5
Concentration (µmolL-1)
time (h)
0
20
40
60
80
100
0
500
1000
1500

Figure 1d

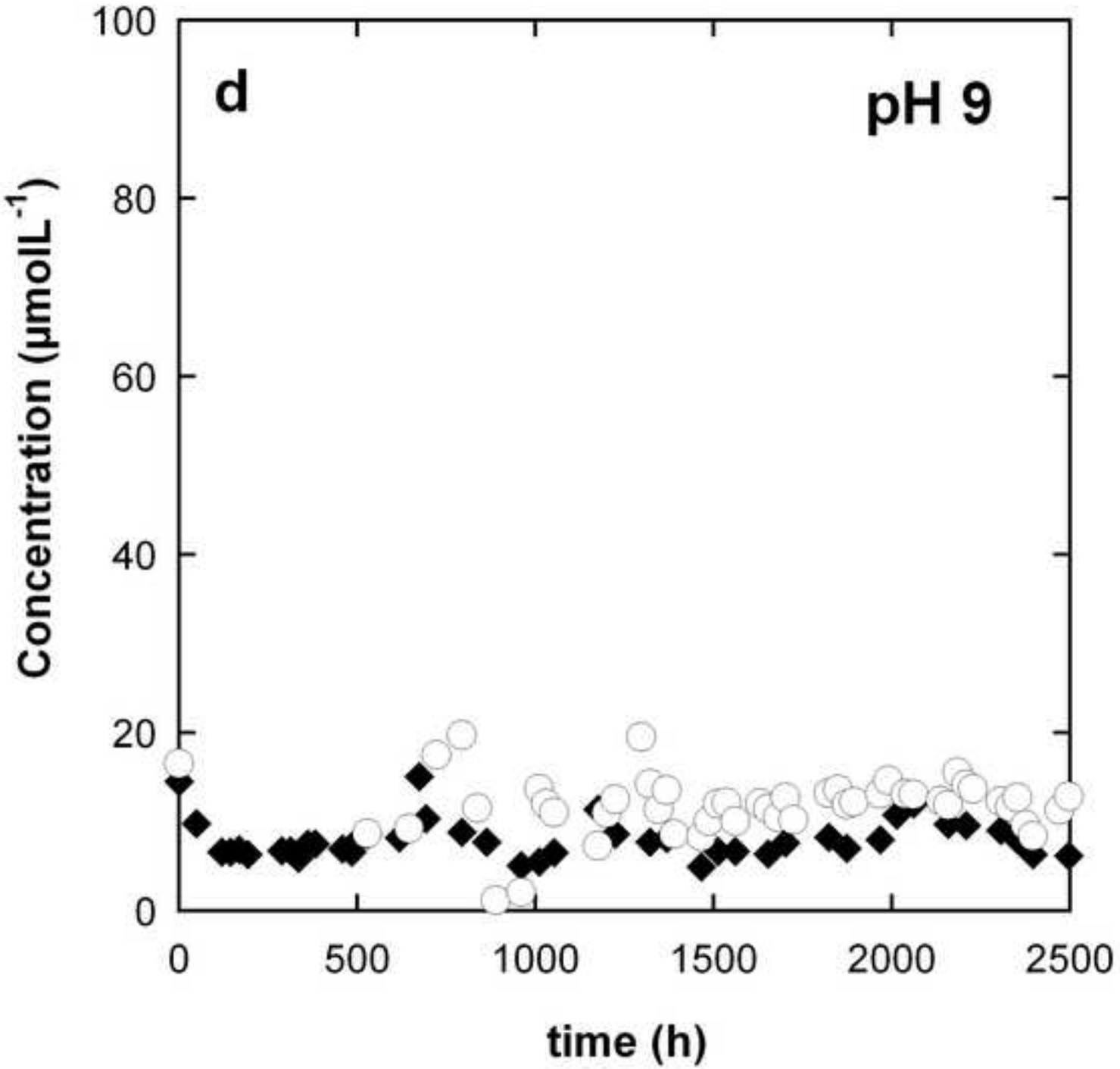
d
pH 9
Concentration (µmolL-1)
100
80
60
40
20
0
0
500
1000
1500
2000
2500
time (h)

Figure 2

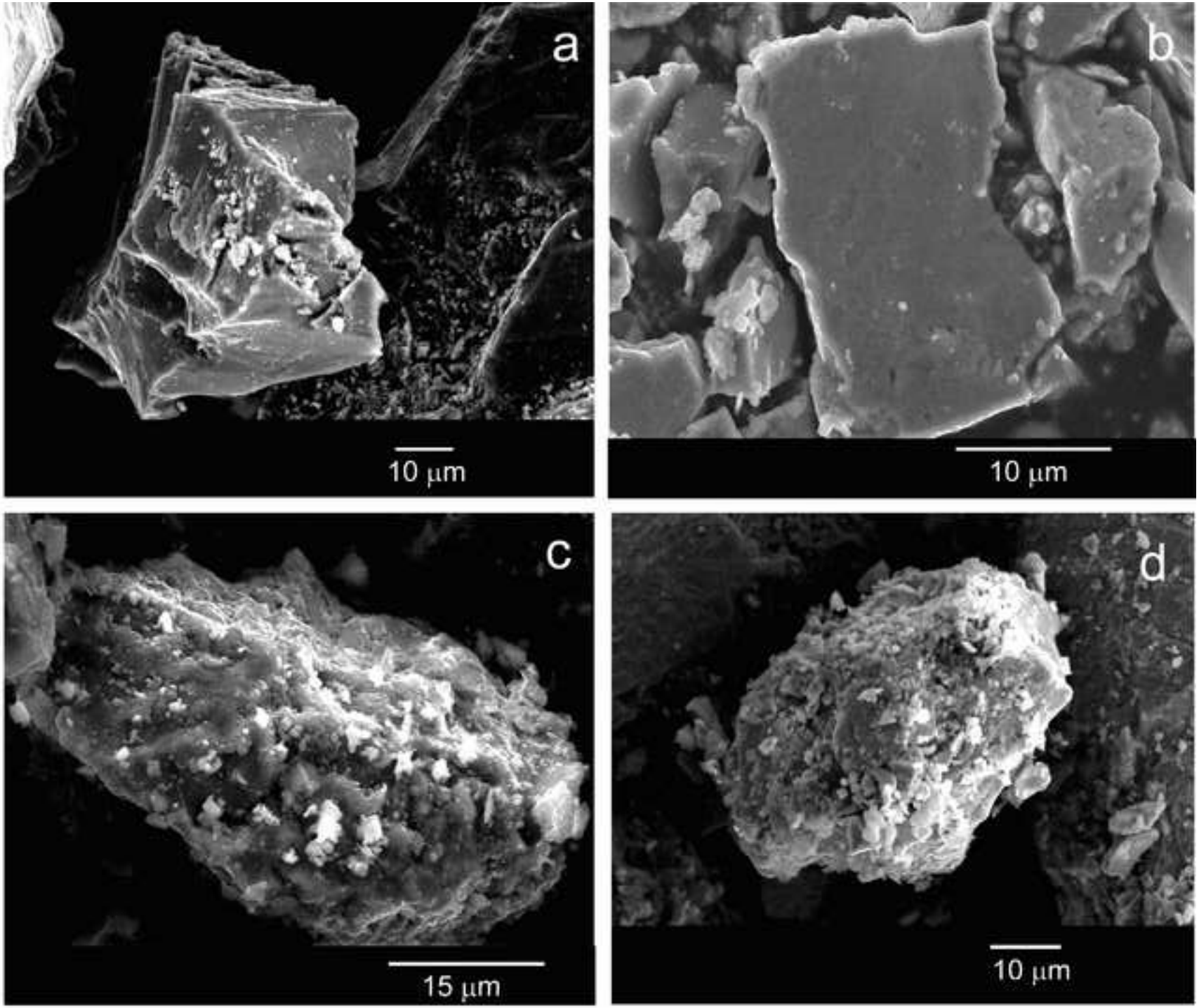

Figure 3

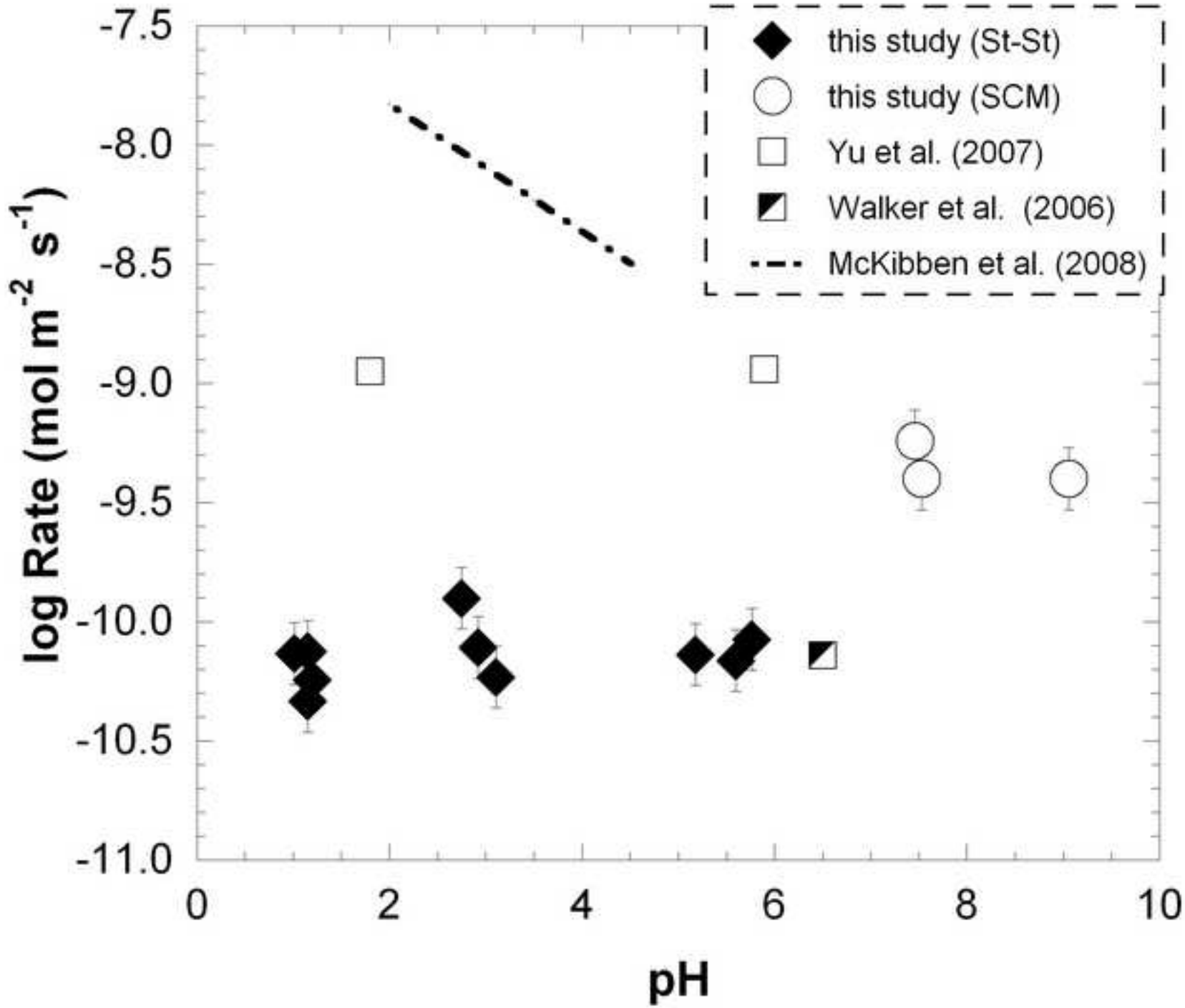
this study (St-St)
this study (SCM)
Yu et al. (2007)
Walker et al. (2006)
McKibben et al. (2008)
log Rate (mol m-2 s-1)
-7.5
-8.0
-8.5
-9.0
-9.5
-10.0
-10.5
-11.0
0
2
4
6
8
10
pH

Figure 4a

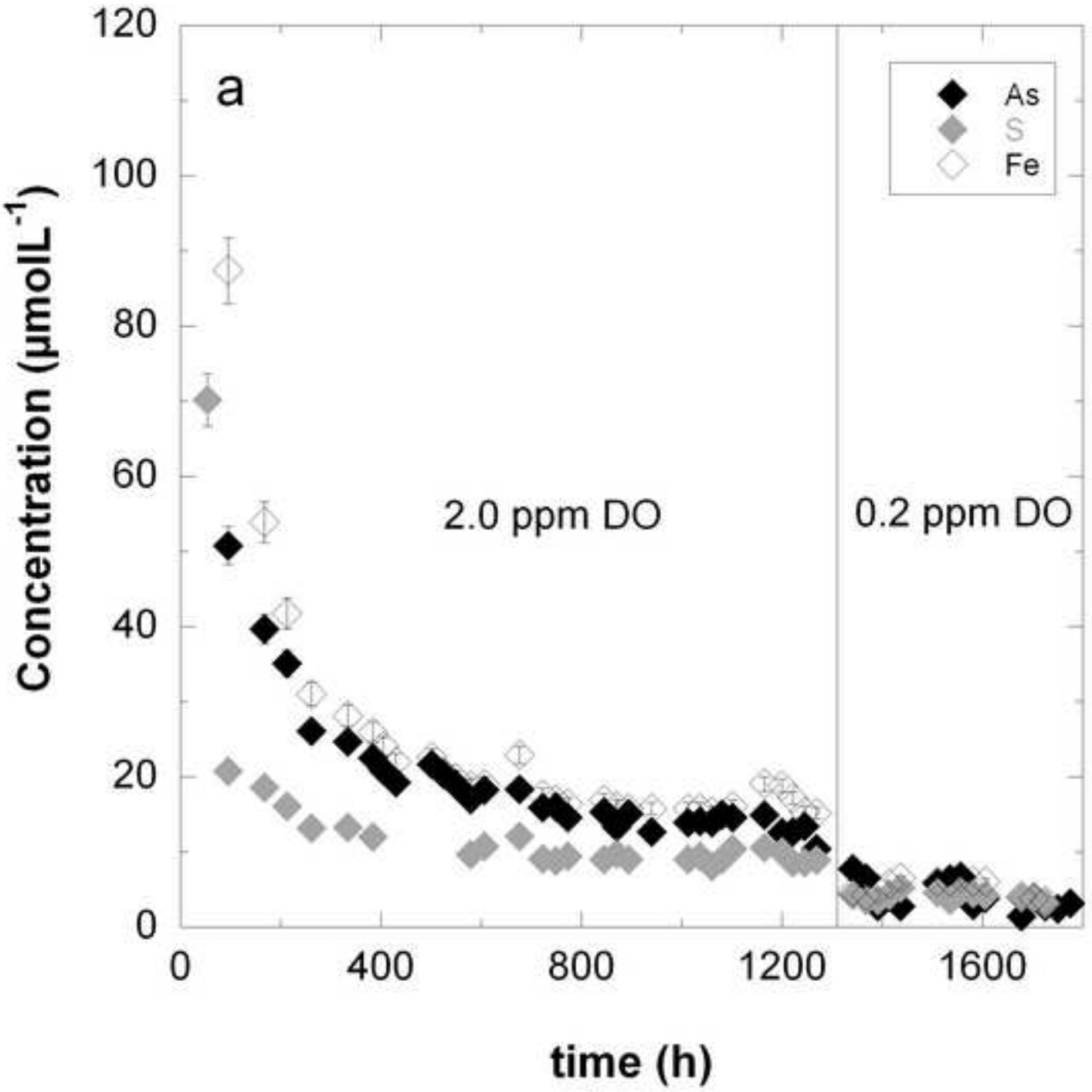
a
As
S
Fe
2.0 ppm DO
0.2 ppm DO
Concentration (μmolL-1)
time (h)
0
20
40
60
80
100
120
0
400
800
1200
1600

Figure 4b

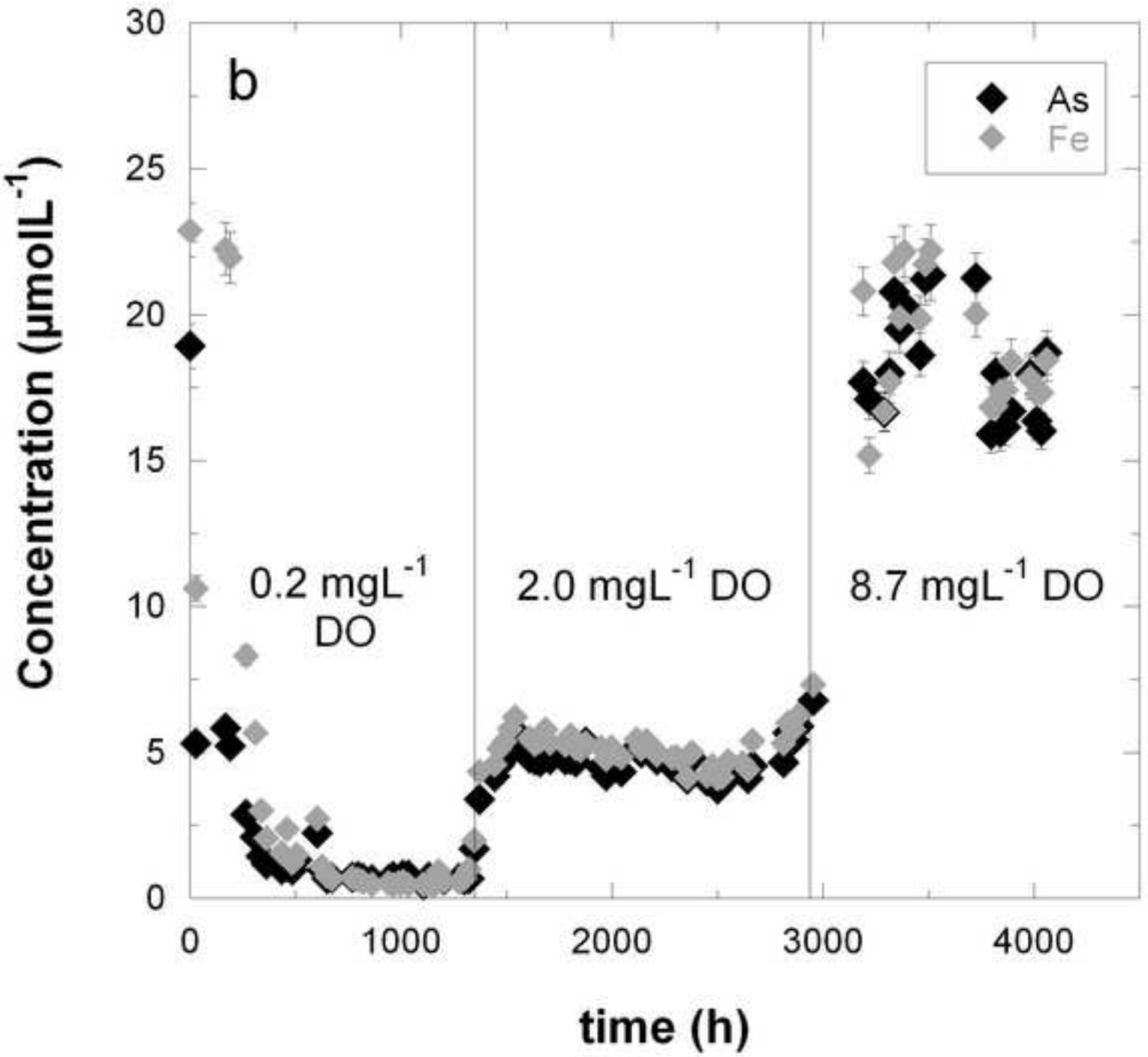
b
As
Fe
0.2 mgL-1 DO
2.0 mgL-1 DO
8.7 mgL-1 DO
Concentration (µmolL-1)
time (h)
0
5
10
15
20
25
30
0
1000
2000
3000
4000

Figure 5a

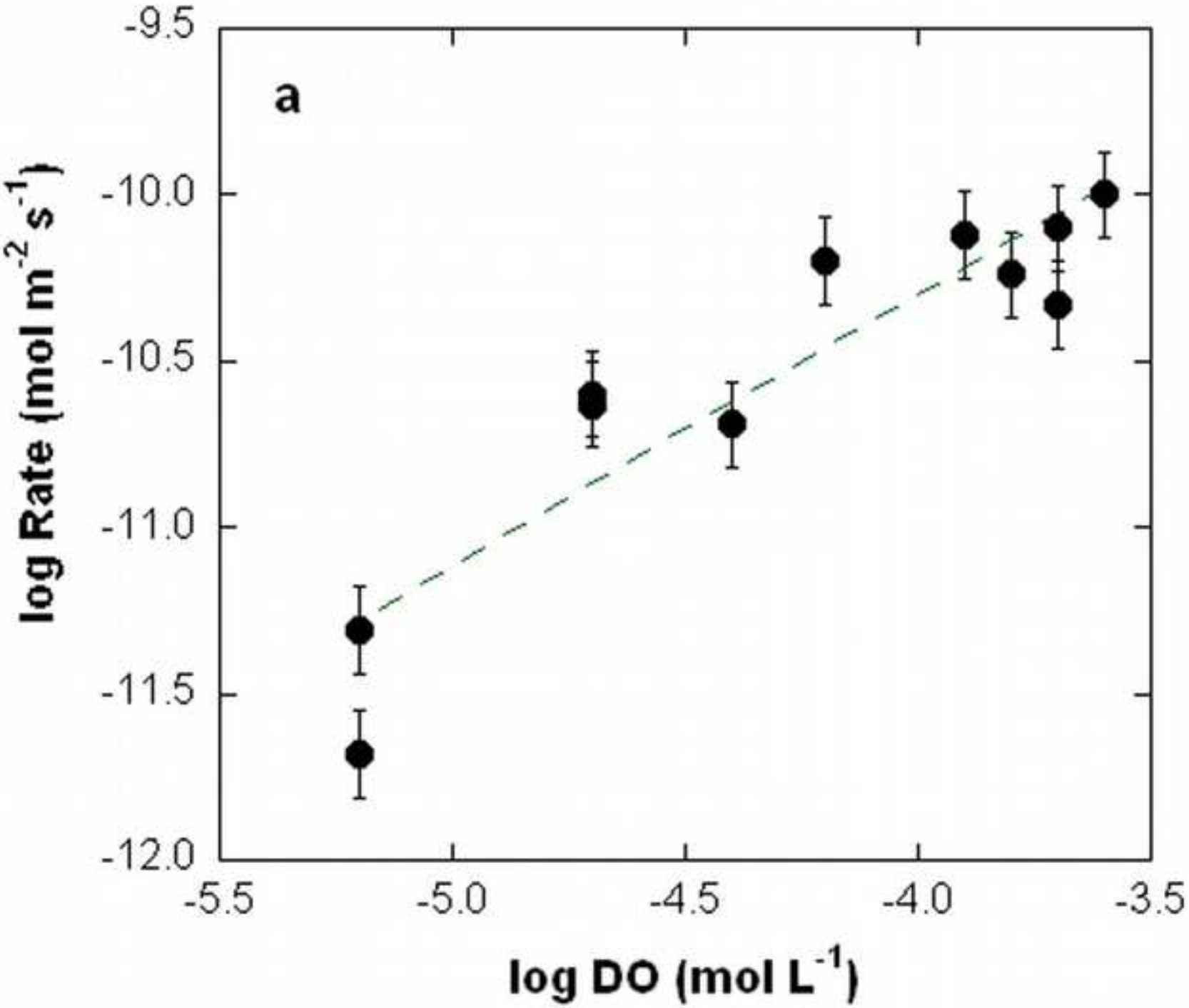
a
-9.5
-10.0
-10.5
-11.0
-11.5
-12.0
-5.5
-5.0
-4.5
-4.0
-3.5
log Rate (mol m-2 s-1)
log DO (mol L-1)

Figure 5b

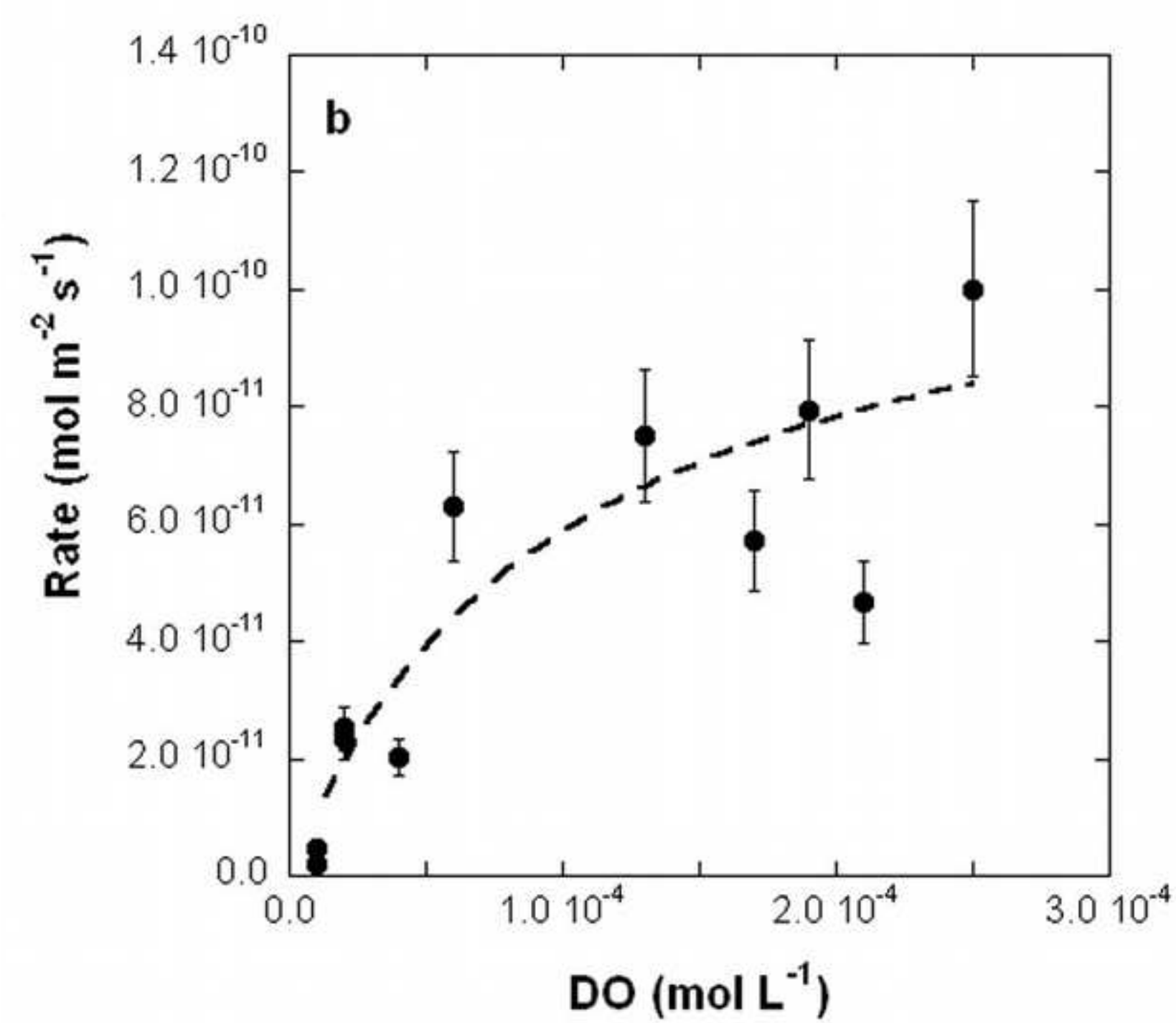
b
Rate (mol m-2 s-1)
1.4 10-10
1.2 10-10
1.0 10-10
8.0 10-11
6.0 10-11
4.0 10-11
2.0 10-11
0.0
0.0
1.0 10-4
2.0 10-4
3.0 10-4
DO (mol L-1)

Figure 6

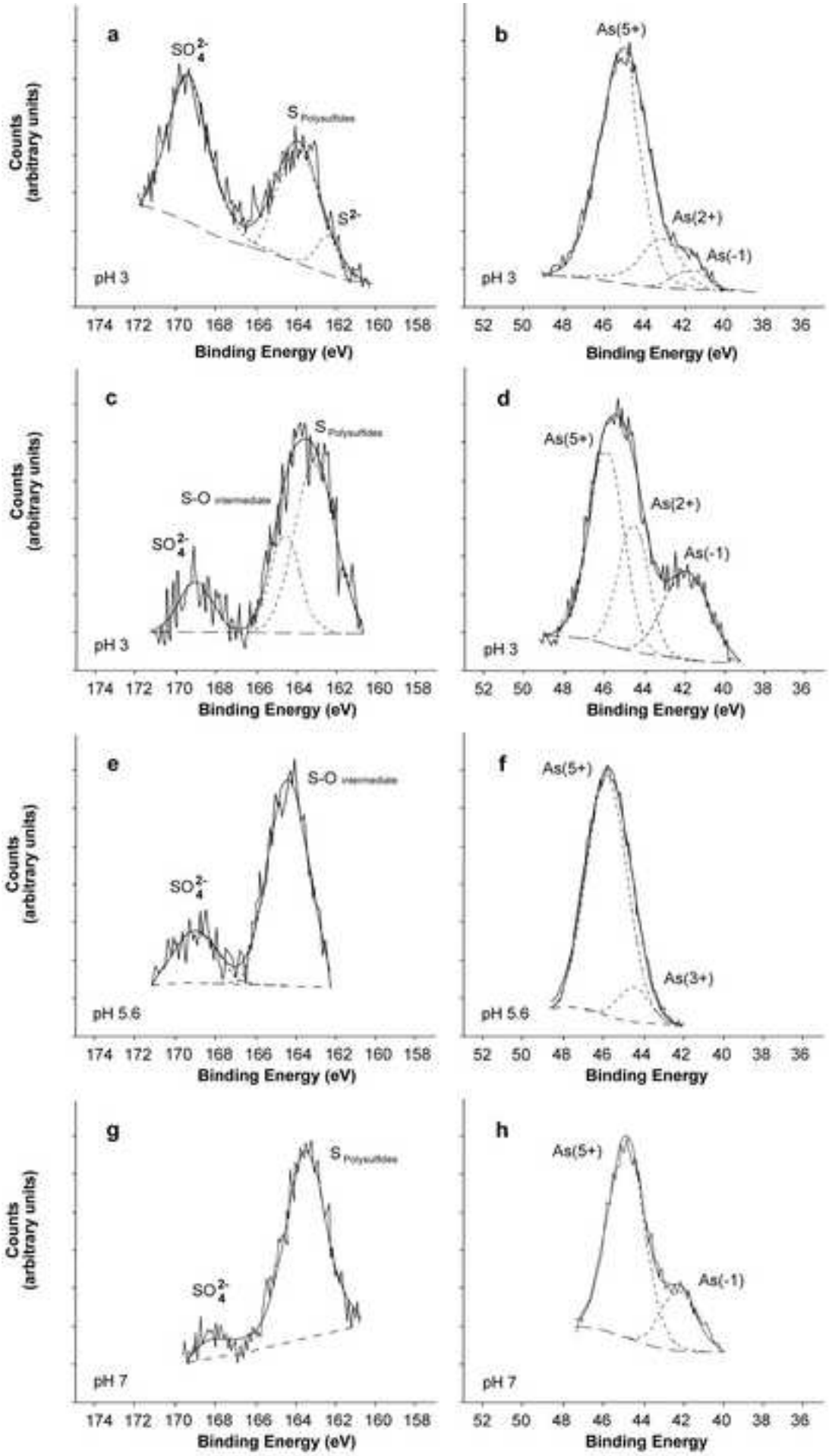
a
SO_4^{2-}
$S_{Polysulfides}$
S^{2-}
pH 3
b
As(5+)
As(2+)
As(-1)
pH 3
c
$S_{Polysulfides}$
S-O intermediate
SO_4^{2-}
pH 3
d
As(5+)
As(2+)
As(-1)
pH 3
e
S-O intermediate
SO_4^{2-}
pH 5.6
f
As(5+)
As(3+)
pH 5.6
g
$S_{Polysulfides}$
SO_4^{2-}
pH 7
h
As(5+)
As(-1)
pH 7
Counts (arbitrary units)
174 172 170 168 166 164 162 160 158
52 50 48 46 44 42 40 38 36
Binding Energy (eV)

Figure 7

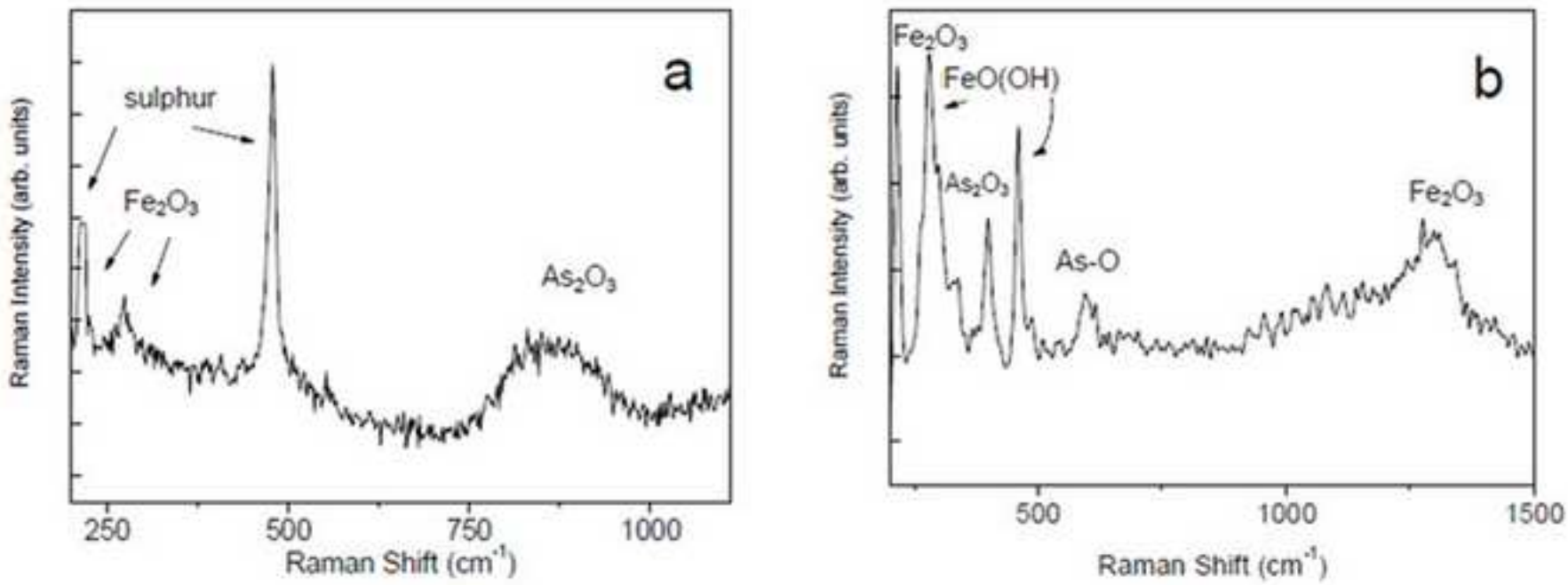
a
sulphur
Fe_2O_3
As_2O_3
Raman Intensity (arb. units)
250
500
750
1000
Raman Shift (cm^{-1})
b
Fe_2O_3
FeO(OH)
As_2O_3
As-O
Fe_2O_3
Raman Intensity (arb. units)
500
1000
1500
Raman Shift (cm^{-1})

Figure 8

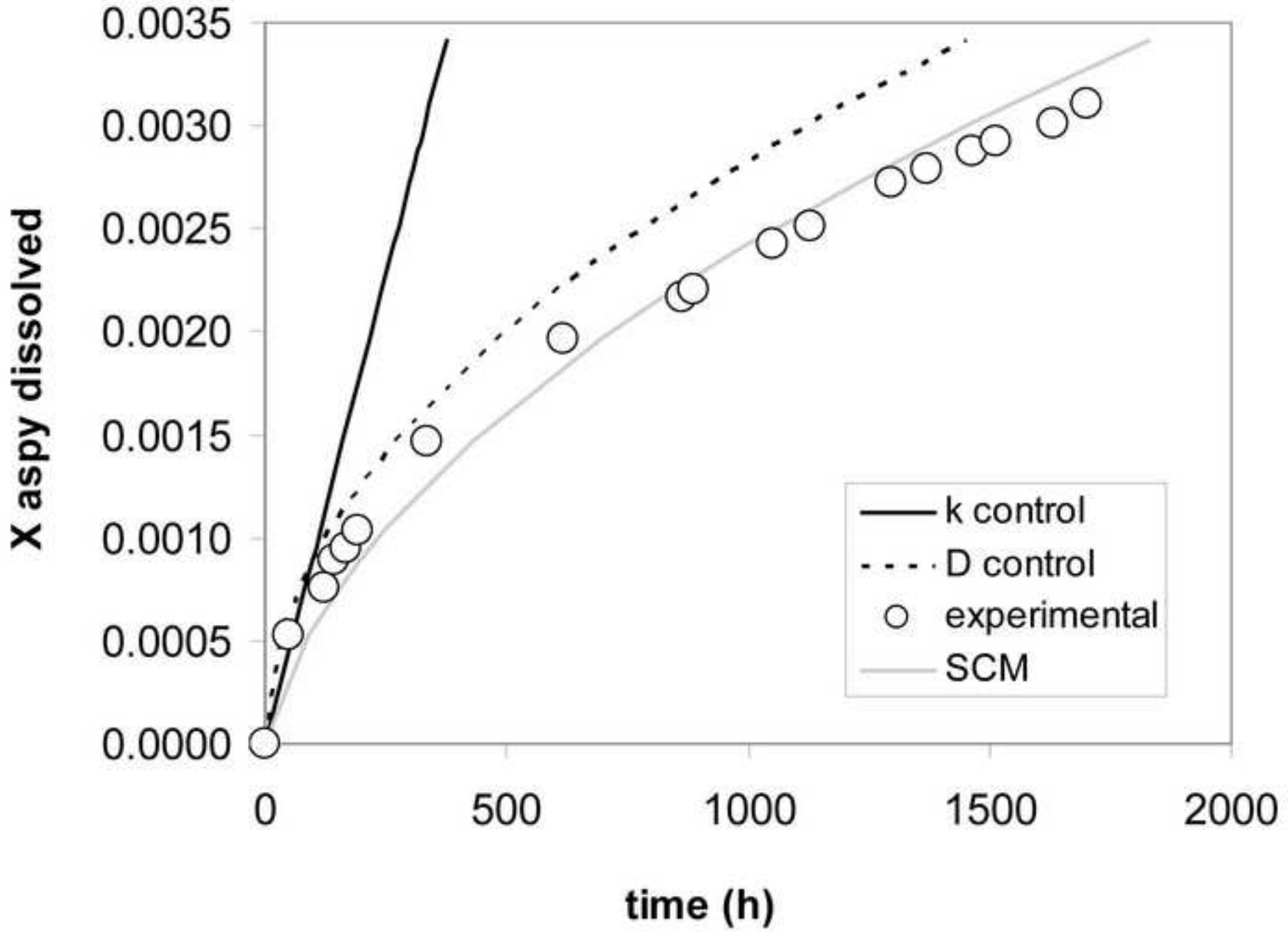
0.0035
0.0030
0.0025
0.0020
0.0015
0.0010
0.0005
0.0000
X aspy dissolved
0
500
1000
1500
2000
time (h)
k control
D control
experimental
SCM

Figure 9

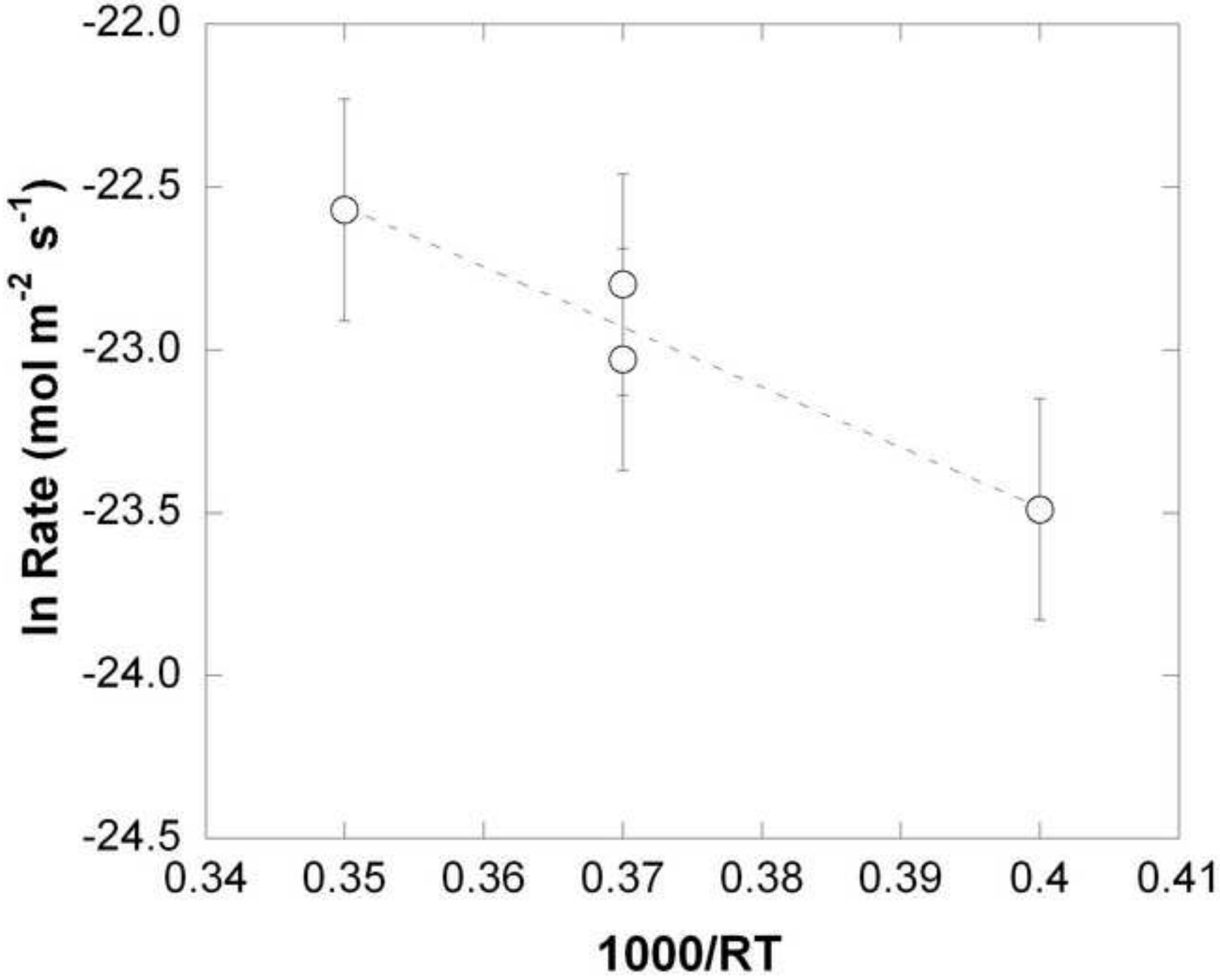
-22.0
-22.5
-23.0
-23.5
-24.0
-24.5
ln Rate (mol m-2 s-1)
0.34
0.35
0.36
0.37
0.38
0.39
0.4
0.41
1000/RT

Table 1

Experiment	Stirring	Electrolyte	Flow rate	pH	logDO input	logDO calculated	T	S	Fe	As	Stoichiometry			Final BET	initial mass	final mass	R_{As}	log R_{As}	R_{Fe}	log R_{Fe}
			(mL min^{-1})		(mol L^{-1})		(°C)		(μM)		Fe/As	S/As	Fe/S	(m^2 g^{-1})	(g)		(mol m^{-2} s^{-1})			
ASP-1	no	H_2SO_4	0.040	1.0	-3.6	3.7	25	99877	32.76	29.38	1.1	-	-	0.54	0.5014	0.4875	$7.4 \cdot 10^{-11}$	-10.1	$8.2 \cdot 10^{-11}$	-10.1
ASP-2	no	H_2SO_4	0.040	2.7	-3.6	3.8	25	963	41.34	34.66	1.1	-	-	0.40	0.5028	0.4962	$1.3 \cdot 10^{-10}$	-9.9	$1.4 \cdot 10^{-10}$	-9.9
ASP-3	no	HCl	0.037	1.2	-3.6	3.8	25	18.37	38.43	34.50	1.1	0.5	2.1	0.67	0.5039	0.4912	$5.7 \cdot 10^{-11}$	-10.2	$6.2 \cdot 10^{-11}$	-10.2
ASP-4	no	HCl	0.038	3.1	-3.6	3.7	25	18.37	30.96	29.67	1.0	0.6	1.7	0.65	0.5076	0.4930	$5.9 \cdot 10^{-11}$	-10.2	$6.1 \cdot 10^{-11}$	-10.2
ASP-5	yes	HCl	0.041	1.1	-3.6	3.9 [a]	25	27.76	53.97	50.33	1.1	0.5	1.9	0.63	0.8002	0.7330	$7.5 \cdot 10^{-11}$	-10.1	$8.1 \cdot 10^{-11}$	-10.1
ASP-7	no	HCl	0.034	1.3	-4.2	-4.4	25	4.34	9.16	7.69	1.2	0.6	1.2	0.43	0.5034	0.5013	$2.0 \cdot 10^{-11}$	-10.7	$2.4 \cdot 10^{-11}$	-10.6
ASP-8	no	HCl	0.036	3.1	-4.2	-4.8 [b]	25	22.69	22.51	17.42	1.3	1.3	1.0	0.60	0.7991	0.7911	$2.2 \cdot 10^{-11}$	-10.7	$2.8 \cdot 10^{-11}$	-10.6
ASP-9	no	HCl	0.038	1.1	-4.2	-4.7 [b]	25	22.93	18.89	15.64	1.2	1.0	0.8	0.49	0.8068	0.7992	$2.5 \cdot 10^{-11}$	-10.6	$3.0 \cdot 10^{-11}$	-10.5
ASP-10	no	Fe^{2+}&H_2SO_4	0.038	1.2	-4.2	-3.7	25	124520	10070	21.49	-	-	-	0.61	0.4937	0.4829	$4.7 \cdot 10^{-11}$	-10.3	-	-
ASP-11	no	HCl	0.014	1.1	-5.2	-5.4 [c]	25	9.81	7.83	4.38	1.8	1.7	0.8	0.33	0.8090	0.8075	$2.1 \cdot 10^{-12}$	-11.7	$3.7 \cdot 10^{-12}$	-11.4
ASP-12-a	yes	HCl	0.046	1.2	-4.2	-4.7 [b]	25	8.89	16.38	14.60	1.1	0.6	1.8	0.48	0.8239	0.8121	$2.3 \cdot 10^{-11}$	-10.6	$2.6 \cdot 10^{-11}$	-10.6
ASP-12-b	yes	HCl	0.048	1.3	-5.2	-5.4 [c]	25	3.89	4.38	3.03	1.1	1.3	1.1	0.48	0.8239	0.8085	$4.9 \cdot 10^{-12}$	-11.3	$7.0 \cdot 10^{-12}$	-11.2
ASP-50-1	no	HCl	0.033	1.1	-3.6	-3.9	50	29.12	54.27	51.84	1.0	0.6	1.9	0.46	0.5016	0.4742	$1.3 \cdot 10^{-10}$	-9.9	$1.3 \cdot 10^{-10}$	-9.9
ASP-50-2	no	HCl	0.035	2.9	-3.6	-3.9	50	48.38	71.67	78.72	1.0	0.6	1.5	0.51	0.8037	0.7763	$1.2 \cdot 10^{-10}$	-9.9	$1.1 \cdot 10^{-10}$	-10.0
ASP-70-1	no	HCl	0.037	1.0	-3.6	-3.7	70	28.01	59.06	49.19	1.2	0.9	2.1	0.41	0.5011	0.4785	$1.4 \cdot 10^{-10}$	-9.8	$1.7 \cdot 10^{-10}$	-9.8
ASP-13	no	HCl	0.038	5.2	-3.6	-3.8	25	36.90	25.93	33.72	0.8	1.1	0.7	0.63	0.5066	0.4702	$7.3 \cdot 10^{-11}$	-10.1	$5.6 \cdot 10^{-11}$	-10.3
ASP-14	no	DDW	0.036	5.5	-3.6	-3.7	25	15.45	4.06	18.03	0.2	0.8	0.3	0.67	0.5023	0.4851	$3.2 \cdot 10^{-11}$	-10.5	$7.3 \cdot 10^{-12}$	-11.1
ASP-15	yes	DDW	0.035	5.8	-3.6	-4.1	25	91.24	35.05	66.12	0.5	1.4	0.4	0.59	0.8039	0.7754	$8.4 \cdot 10^{-11}$	-10.1	$4.5 \cdot 10^{-11}$	-10.3
ASP-16-a	no	DDW	0.040	5.6	-5.2	-5.6	25	4.80	0.62	1.30	0.5	2.2	0.1	0.61	0.8033	0.8024	$1.7 \cdot 10^{-12}$	-11.8	$8.4 \cdot 10^{-13}$	-12.1
ASP-16-b	no	DDW	0.033	5.6	-3.6	-4.0	25	71.11	15.24	60.41	0.3	1.2	0.2	0.61	0.8033	0.7875	$6.9 \cdot 10^{-11}$	-10.2	$1.7 \cdot 10^{-11}$	-10.8
ASP-17	no	DDW	0.030	4.4	-3.6	-3.9	70	61.51	23.98	47.43	0.5	1.3	0.4	0.65	0.8002	0.7796	$4.6 \cdot 10^{-11}$	-10.3	$2.3 \cdot 10^{-11}$	-10.6
ASP-18	no	HCl	0.343	1.3	-3.6	-3.6	25	3.19	8.20	9.86	1.2	0.4	3.1	0.61	0.7664	0.7444	$1.0 \cdot 10^{-10}$	-10.0	$1.2 \cdot 10^{-10}$	-9.9
ASP-19	no	HCl	0.176	1.2	-3.6	-3.6	25	6.03	14.09	10.80	0.8	0.4	1.8	0.46	0.7065	0.6772	$1.0 \cdot 10^{-10}$	-10.0	$1.3 \cdot 10^{-11}$	-9.9
ASP-20	no	HCl	0.380	3.0	-4.2	-4.2	25	*b.d.l.*	9.37	8.30	0.9	-	-	0.60	0.8380	0.8092	$1.1 \cdot 10^{-10}$	-10.0	$1.2 \cdot 10^{-10}$	-9.9
ASP-21	no	HCl	0.403	1.0	-4.2	-4.2	25	*b.d.l.*	2.62	2.55	1.0	-	-	0.34	0.8171	0.8076	$6.3 \cdot 10^{-11}$	-10.2	$6.5 \cdot 10^{-11}$	-10.2

b.d.l.: below detection limit

n.c.: not calculated

(a) Log DO measured in the Steady State under the same experimental conditions = -3.8 ± 0.1

(b) Log DO measured in the Steady State under the same experimental conditions = -4.7 ± 0.1

(c) Log DO measured in the Steady State under the same experimental conditions = -5.5 ± 0.1

Table 2

Experiment	Stirring	Electrolyte	Flow rate	pH	logDO		T	initial mass	final mass	R_S	log R_S	D
					input	calculated						
			(mL min^{-1})		(mol L^{-1})		(°C)	(g)		(mol m^{-2} s^{-1})		(m^{-2} s^{-1})
ASP-22	no	KH_2PO_4	0.034	7.5	-3.6	-3.6	25	0.5027	0.5005	$4.0 \cdot 10^{-10}$	-9.4	$1.0 \cdot 10^{-17}$
ASP-23	yes	KH2PO4	0.036	7.5	-3.6	-3.7	25	0.8040	0.7957	$5.6 \cdot 10^{-10}$	-9.2	$7.0 \cdot 10^{-16}$
ASP-24	no	$Na_2B_4O_7$	0.031	9.1	-3.6	-3.7	25	0.5064	0.5014	$4.0 \cdot 10^{-10}$	-9.4	$1.5 \cdot 10^{-16}$
ASP-25	yes	$Na_2B_4O_7$	0.032	8.9	-3.6	-3.6	25	0.8040	0.7925	Do not fit SCM		Do not fit SCM

Table 3

Sample	pH	S	Fe (at. %) †	As	Fe/S	As/S	Fe/As
Initial FeAsS		*33.0*	*33.0*	*33.0*	*1*	*1*	*1*
ASP-25-1*	1.0	35.9	26.2	36.7	0.73	1.02	0.71
ASP-25-3	1.2	37.5	27.5	34.2	0.73	0.91	0.80
ASP-25-2*	2.7	35.1	20.7	42.1	0.59	1.20	0.49
ASP-25-4	3.1	34.7	28.7	35.6	0.83	1.03	0.81
ASP-25-23	5.8	17.2	41.4	38.4	2.40	2.23	1.08
ASP-25-11	9.1	33.8	47.4	18.9	1.40	0.56	2.51

† *Estimated normalizing out the rest of elements (oxygen and adventicious carbon)*

* *Experiments carried out in H_2SO_4 solutions*

Table 4

Raw	pH 3	pH 7
AsFeS [1,2]	AsFeS [1,2]	AsFeS [1,2]
AsFeS [1,2]	As_2O_3 [3,4]	$As_2O_3 + Fe_2O_3$ [3,4,5]
AsFeS [1,2]	AsFeS [1,2]	AsFeS [1,2]
AsFeS [1,2]	Fe_2O_3 [5]	AsFeS [1,2]
SiO_2	AsFeS+S [1,2,5]	As_2O_3 [3,4]
AsFeS [1,2]	AsFeS +As_2O_3 [3,4]	As_2O_3 [3,4]
AsFeS [1,2]	AsFeS [1,2]	AsFeS [1,2]
AsFeS [1,2]	Fe_2O_3+AsO_4+S [3,4,5,6,7]	AsFeS [1,2]

(1) McGuire et al. (2001b);

(2) Costa et al. (2002);(3) Martens et al. (2003a);

(4) Flynn et al. (1976); (5) Bersani et al. (1999);

(6) Mycroft et al. (1990);(7) Martens et al. (2003b).

Table 5

	Experiment type	pH	Temp (°C)	DO (mgL^{-1})	Activation Energy ($kJ\ mol^{-1}$)	Dissolution Rate ($mol\ m^{-2}\ s^{-1}$)	Duration experiment (h)
Walker et al. (2006)	Mixed flow reactor	6.3-6.7	25	0.3-17	-	$r=10^{-10.14\pm0.03}$	30
McKibben et al. (2008)	Batch reactor	2-5	10-40	-	-	$r = 10^{-6.11}[O_{2(aq)}]^{0.33(\pm0.18)}\ a_{H+}{}^{0.27(\pm0.09)}$	-
Yu et al. (2007)	Mixed flow reactor	1.8-6.4	15-45	0.2-24.6	57	$r=10^{(-2211\pm57)/T}\ [O_{2(aq)}]^{0.45\ (\pm0.05)}$	6-8
This study	Flow through reactor	1-6	25-70	0-8.7	18.5	$r = 10^{-7.41\ (\pm0.47)}\ [O_{2(aq)}]^{0.78(\pm0.11)}\ a_{H+}{}^{-0.12(\pm0.07)}$	600-4500